# Isobars and the medium-energy $(\gamma,p)$ reaction*

J. T. Londergan
*Department of Physics, Indiana University, Bloomington, Indiana 47401*

G. D. Nixon
*Department of Physics, Indiana University, and Center for Theoretical Physics, M.I.T., † Cambridge, Massachusetts 02138*

(Received 19 June 1978; revised manuscript received 7 November 1978)

Recently, precise experimental measurements have been obtained for the reaction $^{16}O(\gamma,p)^{15}N$ for photon energies 50–350 MeV. For photon energies greater than 100 MeV, isobar photoproduction is expected to provide an important part of the $(\gamma,p_0)$ reaction. We evaluate the isobar contribution to the $(\gamma,p)$ reaction, and we add this amplitude to a term which corresponds to direct knockout of the proton by the photon. We compare our results in detail with the experimental data from Glasgow and Bates on $^{16}O$. Our calculation uses coupling constants and nuclear wave functions determined from independent experiments, and we neglect the isobar-nucleus interaction. Agreement with the experimental data is quite reasonable, and isobar photoproduction provides a very large contribution to the nuclear photoeffect in $^{16}O$, for photon energies above about 100 MeV. We consider the effects of various corrections to our formalism, such as the effect of distortion of the outgoing nucleon by the nuclear force, center of mass corrections, and the inclusion of $\rho$ mesons in addition to pions at the isobar decay vertex. None of these corrections alters the qualitative features of the isobar amplitude and its importance in the nuclear photoeffect at medium energies.

[NUCLEAR REACTIONS, photonuclear reactions, nuclear photoeffect, medium energies, isobars, isobar current, $(\gamma,p)$ reactions.]

## I. INTRODUCTION

In this paper we consider the contribution of various amplitudes to the $(\gamma,p)$ reaction at medium energies. Several experiments have been carried out on 1$s$-shell[1-22] and 1$p$-shell nuclei[23-42] for photon energies up to 400 MeV. Recently, $(\gamma,p)$ experiments have been carried out at Glasgow, in which cross sections were obtained for discrete final states (or groups of low-lying excited states) of the residual nucleus.[25,26,37-40] High-quality data were obtained for photon energies from 40–100 MeV, and it has been argued that these data allow an extraction of the single-particle momentum density distribution of the ejected nucleon.[39,40,42] Additional experiments on heavier nuclei are presently being carried out in this energy region at Glasgow.[43] At the Bates linac, the reaction $^{16}O(\gamma,p_0)^{15}N$ (leading to the ground state of $^{15}N$) has been studied for photon energies 100–350 MeV.[41-43]

The simplest picture of the photonuclear reaction, the "direct reaction" mechanism, is one in which an individual nucleon is struck by a photon and ejected from the nucleus. In this process, one evaluates the nuclear matrix elements of the one-body part of the electromagnetic operator, and the final-state nucleon-nucleus interaction can be estimated by using distorted waves for the outgoing nucleon wave function. In addition to this term, we expect to obtain contributions from exchange-current effects in which the photon is absorbed by two or more interacting nucleons. The relative contribution from exchange currents should increase as the photon energy increases, since the direct reaction requires progressively larger momentum components of the single-particle wave functions. In this paper, we will restrict ourselves to consideration of the isobar current. The $\Delta(1232)$, a nucleon excitation at about 300 MeV with a free width of about 115 MeV,[44] will contribute to photonuclear reactions over a rather wide range of photon energies spanning the "isobar-production" region. Effects of isobar production by electromagnetic currents are seen in quasielastic electron scattering, where isobar electroproduction produces a sharp peak in the nuclear response function.[45-47] The isobar current will undoubtedly contribute in some way to $(\gamma,p)$ reactions leading to discrete final nuclear states, although in contrast to the inclusive quasielastic processes the isobar current will be modulated by single-particle momentum wave functions. The questions we shall discuss in this paper are as follows: (i) Is the isobar contribution significant compared with the direct-reaction contribution at these energies? (ii) What is the "signature" for the isobar photoproduction amplitude, and how well does the isobar contribution reproduce the experimental $(\gamma,p)$ cross sections? (iii) How reliably can we calculate this term using coupling constants and nuclear form factors determined from independent experiments?

In a previous paper (hereafter called I),[48] we reported preliminary results of a calculation which

 

indicated that isobar [$\Delta(1232)$] formation and decay might provide a sizeable contribution to the nuclear photoeffect, for photon energies of 100 MeV and higher. In I, we used a simple plane-wave model for the direct term and we made several simplifications designed to give at least a qualitative picture of the isobar current and its significance in medium-energy $(\gamma,p)$ reactions. In this paper we present a considerably more detailed exposition of both the direct reaction and isobar amplitudes, and we compare our results with the extensive $(\gamma,p)$ data on $^{16}$O from 40–400 MeV. We shall demonstrate that the isobar contribution seems to be very important, at least for photon energies of 100 MeV and higher, and that it produces reasonable quantitative agreement with existing data.

In Sec. II of this paper we will review the plane-wave impulse approximation (PWIA) for the $(\gamma,p)$ reaction leading to discrete final states of the residual nucleus. Although such an approximation is surely inadequate as a description of the nuclear photoeffect at medium energies, it provides an extremely simple derivation of several features of the $(\gamma,p)$ reaction which can then be compared and contrasted with more sophisticated calculations and with experimental data. As is well known, in PWIA the laboratory differential cross section for $(\gamma,p)$ reactions is directly proportional to the square of the proton bound state wave function evaluated at momentum $\vec{q}=\vec{k}_N-\vec{k}_\gamma$, where $\vec{k}_N$ is the outgoing proton lab momentum and $\vec{k}_\gamma$ is the incident photon momentum. The possibility of directly measuring the single-particle momentum components through the $(\gamma,p)$ reaction provided a motivation for earlier experimental and theoretical investigations. This reaction also gave the promise of measuring the relatively poorly known high momentum components in the single-particle wave function. In the $(\gamma,p)$ reaction the photon transfers nearly all its energy to the proton; consequently the outgoing proton will have a considerably larger momentum than the photon, so that the magnitude of $\vec{q}$ will be large. If the PWIA predictions were correct, then the $(\gamma,p)$ cross sections would provide a direct measurement of the momentum density for the single-particle wave function far above the Fermi momentum. We will review the PWIA cross sections predicted for different choices of single-particle wave functions in Sec. II.

In order to account for the nuclear forces in a realistic manner, the simple PWIA analysis of the reaction must be modified. The first correction we consider is the final-state interaction of the outgoing proton, and in Sec. III we discuss a modification of the proton wave function which approximates the proton distorted waves as generated from phenomenological optical potentials. We want to use the same distorted waves for the direct reaction and isobar amplitudes, which restricts us to fairly simple forms for the approximate wave functions in view of the computer time required to evaluate the isobar current. The method we have chosen is an extension to medium-energy reactions of an approximation studied by McCarthy[49] for nucleon wave functions generated from optical potentials. We discuss in some detail the simplifications which occur at medium energies, relative to the lower-energy analyses of McCarthy, and we demonstrate the quality of our fits to proton distorted waves at energies of 100 MeV and higher.

In Sec. IV, we derive in detail the isobar contribution to medium-energy photonuclear reactions, and we compare our results with the existing experimental data for the $^{16}O(\gamma,p_0)^{15}N$ reaction in this energy region. As our present calculation contains no free parameters, we discuss our choices for various coupling constants, form factors, and nuclear wave functions, all of which are fixed by other experiments. We examine the form of differential cross sections at fixed proton laboratory angle vs photon energy, we predict the form of the cross sections at fixed photon energy vs proton lab angle, and we discuss briefly the possibility of measuring the $(\gamma,p)$ cross section to the 6.32 MeV, $\frac{3}{2}$-excited state of $^{15}$N and its usefulness in identifying the reaction mechanism at these energies.

For clarity, we introduce several simplifications in the derivations of Sec. IV; for example, we neglect the effects of nucleon-nucleus final-state interactions and we include only the $\pi$ decay of the isobar and not $\rho$ decay. In Sec. V, we discuss the results of including these terms in the isobar-photoproduction amplitude. In addition, we estimate the effects of c.m. corrections to the shell model wave functions used in our calculations. As we have neglected the change in the isobar propagator due to the isobar-nucleus interaction, we attempt to discuss the sensitivity of our results to self-energy modifications of the isobar propagator. These modifications would presumably be most dramatic to the degree which they changed the isobar width in the nucleus from its free value. Although a precise determination of some of these quantities awaits more extensive theoretical investigations, we shall be able to estimate the extent to which our results are dependent upon the particular choices we have made for several of our parameters.

## II. PWIA ANALYSIS OF THE $(\gamma,p)$ REACTION

The scattering amplitude for the $(\gamma,p)$ reaction can be written as

$$M_{fi}^{\lambda} = -\langle \psi_f | \int d^3x \vec{j}(\vec{x}) \cdot \vec{A}_{\lambda}(\vec{x}) | \psi_i \rangle , \tag{2.1}$$

where $|\psi_i\rangle$ is the initial target wave function for $A$ particles, $|\psi_f\rangle$ is the final-state wave function, $\vec{A}_{\lambda}(\vec{x})$ is the electromagnetic potential of a photon with polarization component $\lambda$ along the polarization axis, and $\vec{j}(x)$ is the nuclear electromagnetic current operator. The final-state wave function $|\psi_f\rangle$ can be written as the product of the residual nucleus with $(A-1)$ particles in state $f$ and a relative proton-nucleus continuum wave function. The photon electromagnetic potential corresponding to polarization component $\lambda$ has the form

$$\vec{A}_{\lambda}(\vec{x}) = 1/(2\omega_{\gamma})^{1/2} e^{(i\vec{k}_{\gamma}\cdot\vec{x})} \epsilon_{\lambda} , \tag{2.2}$$

where $\vec{k}_{\gamma}$ is the photon laboratory momentum and $\omega_{\gamma}$ the photon energy ($\omega_{\gamma} = |\vec{k}_{\gamma}|$).[50]

In general we can expand the nuclear current operator into one-body, two-body, and higher-order components; for the impulse approximation which we consider in this section, it is sufficient to consider the one-body operator only, so that we can write the current in terms of a convective term and a magnetic moment term

$$\vec{j}_1(\vec{x}) = -e \sum_{j=1}^{A} \left\{ \frac{e_j}{2iM} [\delta(\vec{r}_j - \vec{x})\vec{\nabla}]_{SYM} - \delta(\vec{r}_j - \vec{x}) \frac{\mu_j}{2M} \sigma(\vec{j}) x \vec{\nabla} \right\} . \tag{2.3}$$

In Eq. (2.3), $M$ is the nucleon mass, $e_j$ is the charge of the $j$th nucleon, and $\mu_j$ is the magnetic moment of the nucleon in nuclear magnetons. We use the notation

$$[\delta(\vec{r}_j - \vec{x})\vec{\nabla}]_{SYM} \equiv \delta(\vec{r}_j - \vec{x})(\vec{\nabla}_j - \vec{\nabla}_j) . \tag{2.4}$$

For the nucleon effective charge we use 0 for neutrons and 1 for protons.[51]

Evaluation of the matrix elements of Eq. (2.3) is greatly simplified if we use a plane wave for the outgoing nucleon wave function; that is, if we neglect all interactions of the nucleon subsequent to its ejection by the photon. In that case we can integrate by parts to obtain the matrix element

$$M_{fi}^{\lambda} = -e/(2\omega_{\gamma})^{1/2} \sum_{j=1}^{A} \int d\vec{x}_1 \cdots d\vec{x}_A \psi_f^{A-1\dagger}(\vec{x}_1, \ldots \vec{x}_{j-1}, \vec{x}_{j+1}, \ldots, \vec{x}_A) e^{-i(\vec{k}_N - \vec{k}_{\gamma})\cdot\vec{x}_j} \times \chi_N^{\dagger} \left( \frac{e_j}{M} \vec{k}_N \cdot \vec{\epsilon}_{\lambda} + \frac{i\mu_j \vec{k} x \vec{\sigma} \cdot \vec{\epsilon}_{\lambda}}{2M} \right) \psi_i^A(\vec{x}_1, \vec{x}_2, \ldots, \vec{x}_A) . \tag{2.5}$$

In Eq. (2.5) $\vec{k}_N$ is the outgoing nucleon momentum in the laboratory reference frame, and $\chi_N^{\dagger}$ is the spin-isotopic spin vector for this nucleon. If we define the overlap matrix element between initial and final states

$$\varphi_{fi}(\vec{q}) \equiv \int d\vec{x}\, e^{-i\vec{q}\cdot\vec{x}} \langle \psi_f^{A-1} | \psi_i^A \rangle , \tag{2.6}$$

then in terms of this quantity we see that the amplitude can be written as

$$M_{fi}^{\lambda} = -e/(2\omega_{\gamma})^{1/2} \chi_N^{\dagger} \left( \frac{e_N}{M} \vec{k}_N \cdot \vec{\epsilon}_{\lambda} + \frac{i\mu_N \vec{k}_{\gamma} x \vec{\sigma} \cdot \vec{\epsilon}_{\lambda}}{2M} \right) \varphi_{fi}(\vec{k}_N - \vec{k}_{\gamma}) , \tag{2.7}$$

where $e_N$ and $\mu_N$ in Eq. (2.7) are the charge and magnetic moment, respectively, of the ejected nucleon. The single-particle wave function $\varphi_{fi}$ defined from Eq. (2.6) has an explicit dependence upon the bound nucleon spin and isotopic-spin coordinates, so that the photonuclear amplitude $M_{fi}$ is obtained by taking the matrix elements of Eq. (2.7) between spinors for the final outgoing nucleon and the bound nucleon, respectively.

The laboratory differential cross section, averaged over initial photon polarizations and summed over nucleon and residual nucleus polarizations is given by

$$d\sigma = 2\pi \delta(E_f - E_i) \frac{1}{2} \sum_{\lambda} \sum_{S_N, \alpha} |M_{fi}^{\lambda}|^2 \frac{d^3k_N}{(2\pi)^3} \frac{d^3k_R}{(2\pi)^3} , \tag{2.8}$$

where $\vec{k}_N$ and $\vec{k}_R$ are the nucleon and residual nucleus outgoing momenta, respectively, and $S_N$ and $\alpha$ are the final spins. If we assume an independent-particle model of the nucleus, such that the final state is simply a one-hole state relative to the initial state, then we can write

$$|\psi_i^A\rangle = a_{\alpha}^{\dagger} |\psi_f^{A-1}\rangle , \tag{2.9}$$

where $\alpha$ refers to the single-particle quantum numbers ($nlj$, etc.) of the ejected nucleon. In this case Eq. (2.8) becomes

$$\frac{d\sigma}{d\Omega}(\gamma, N) = \frac{e^2}{16\pi^2} \frac{k_N^2}{k_{\gamma}} \frac{dk_N}{dE_f} \frac{(2j+1)}{(2l+1)} \sum_{m} |\varphi_{nljm}(\vec{k}_N - \vec{k}_{\gamma})|^2 \times \left[ \delta_{\tau_N, 1/2} \left( \frac{k_N^2}{M^2} \sin^2\theta + \frac{k_{\gamma}^2}{2M^2} \mu_p^2 \right) + \delta_{\tau_N, -1/2} \frac{k_{\gamma}^2}{2M^2} \mu_n^2 \right] . \tag{2.10}$$

In Eq. (2.10), $E_f$ is the final total energy of the system

$$E_f=(k_N^2+M^2)^{1/2}+[(\vec{k}_\gamma-\vec{k}_N)^2+M_{A-1}^2]^{1/2}.$$

The first term inside the brackets represents the $(\gamma,p)$ cross section and the second term gives the $(\gamma,n)$ cross section.[52]

The PWIA predictions for $(\gamma,N)$ cross sections are quite interesting and we list the important features of this analysis in order to compare with subsequent calculations.

(i) The differential cross section is directly proportional to the square of the single-particle wave function evaluated at momentum $\vec{k}_N-\vec{k}_\gamma$. In fact, we may write the $(\gamma,p)$ cross section as

$$\frac{d\sigma}{d\Omega}(\gamma,p)=C(k_\gamma,q)\frac{1}{(2\pi)^3}\frac{(2j+1)}{(2l+1)}\sum_m|\varphi_{nljm}(\vec{q})|^2, \tag{2.11}$$

where $\vec{q}=\vec{k}_N-\vec{k}_\gamma$ and

$$C(k_\gamma,q)=\frac{\pi e^2}{2}\frac{k_N^2}{k_\gamma}\frac{dk_N}{dE_f}\left(\frac{k_N^2}{M^2}\sin^2\theta+\frac{k_\gamma^2}{2M^2}\mu_p^2\right). \tag{2.12}$$

In this approximation, then, the differential cross section divided by the factor $C$ is just the square of the single-particle wave function, the "single-particle momentum density" evaluated at momentum $q$ [the sum over $m$ in Eq. (2.11) removes all dependence on the direction of $\vec{q}$ so that the result is a function only of the magnitude $|\vec{q}|$]. In addition, this approximation predicts a "scaling" of the cross sections, that is, the quantity $[1/C(k_\gamma,q)]\times(d\sigma/d\Omega)$ should lie on a universal curve when plotted against $q$. We will elaborate on this point in Sec. III when we discuss the modification of these results due to the final-state interaction of the outgoing proton.

(ii) The convective and magnetic terms enter incoherently in the cross section, since the convective term does not change the nucleon spin while the magnetic term is a pure spin-flip amplitude. In Eq. (2.9), for the $(\gamma,p)$ amplitude, the convective operator gives the term proportional to $(k_N^2/M^2)\sin^2\theta$ while the magnetic moment operator is proportional to $(k_\gamma^2/2M^2)\mu_p^2$.

In the PWIA description of $(\gamma,p)$ reactions we may write

$$\frac{d\sigma^{\rm PWIA}}{d\Omega}(\gamma,p)=\sigma_{\rm conv}+\sigma_{\rm magn}, \tag{2.13}$$

where

$$\left.\frac{\sigma_{\rm conv}}{\sigma_{\rm magn}}\right|_{\rm PWIA}=\frac{2k_N^2\sin^2\theta}{k_\gamma^2\mu_p^2}, \tag{2.14}$$

In Table I we present the ratio $\sigma_{\rm conv}/\sigma_{\rm magn}$ predicted by the PWIA; for photon energies above 100 MeV this predicts a fairly large contribution from the magnetic moment term.[53] For scattering angles sufficiently forward or backward of 90°, the magnetic contribution is often larger than the convective.

TABLE I. Ratio of convective to magnetic cross sections in PWIA calculations of the $(\gamma,p)$ reaction. The ratio $\sigma_{\rm conv}/\sigma_{\rm magn}$ is listed for various photon laboratory energies $\omega_\gamma$ and proton laboratory scattering angles $\theta$.

| $\omega_\gamma$ (MeV) \ $\theta_{\rm lab}$ (deg) | $\frac{\sigma_{\rm conv}}{\sigma_{\rm magn}}$ PWIA 45° | 90° | 135° |
|---|---|---|---|
| 100 | 2.11 | 4.10 | 2.00 |
| 150 | 1.50 | 2.93 | 1.43 |
| 200 | 1.19 | 2.28 | 1.10 |
| 250 | 0.99 | 1.89 | 0.91 |
| 300 | 0.84 | 1.62 | 0.77 |
| 350 | 0.75 | 1.42 | 0.67 |
| 400 | 0.67 | 1.27 | 0.60 |

(iii) The $(\gamma,n)$ cross section is proportional to the magnetic moment term only; at photon energies below 100 MeV this would predict $(\gamma,n)$ cross sections to be much smaller than $(\gamma,p)$ cross sections. We will discuss these predictions in somewhat more detail in Sec. III when we consider the inclusion of distorted waves.

As we have mentioned, since the asymptotic nucleon momentum $k_N$ will be considerably larger than the photon momentum, $\vec{q}\equiv\vec{k}_N-\vec{k}_\gamma$ will be quite large. In PWIA, the $(\gamma,p)$ cross sections thus provide directly the high-momentum components of single-particle wave functions. At the large momenta involved, we might expect considerable uncertainty in the single-particle momentum components, even from wave functions that give reasonable agreement with existing experimental data (which is usually sensitive to lower-momentum components). As an illustration of the variation in different wave functions, we plot the momentum densities for three different $1p$-shell proton wave functions in $^{16}$O. We plot the "single-particle momentum density"[55]

$$\Omega(q)\equiv\frac{1}{(2\pi)^3}\frac{(2j+1)}{(2l+1)}\sum_m|\varphi_{nljm}(\vec{q})|^2, \tag{2.15}$$

in Figs. 1 and 2; $\Omega(q)$ is plotted in $(\mathrm{GeV}/c)^{-3}$ vs momentum $q$. The dot-dashed curve in Fig. 1 is the momentum distribution for a $1p$ simple harmonic oscillator wave function with $b=1.77$ fm. Such a wave function contains essentially no high-momentum components, even though the transition

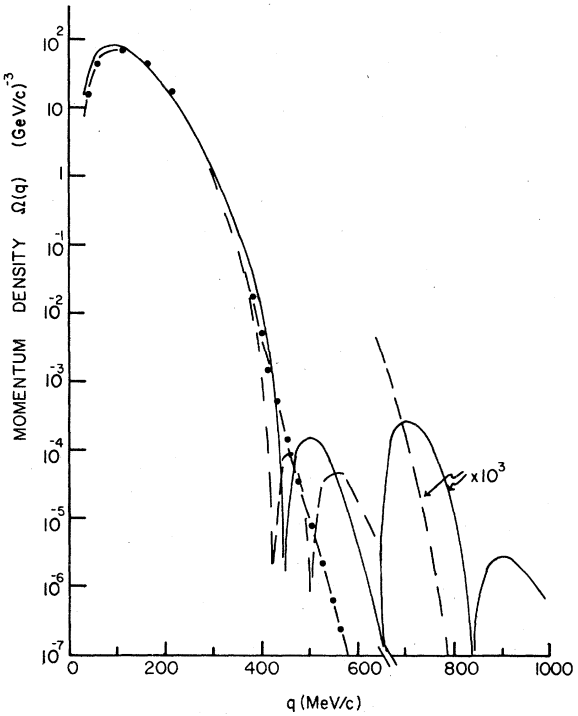


FIG. 1. The single-particle momentum density $\Omega(q)$, in $(\mathrm{GeV}/c)^{-3}$, vs momentum $q$ in MeV/$c$. $\Omega(q)$ is defined in Eq. (2.15); the curves have been calculated for $1p\frac{1}{2}$ protons in $^{16}$O. Solid curve: Elton-Swift wave function (Ref. 51); dashed curve: momentum density obtained from oscillator expansion of Negele's density-dependent Hartree-Fock calculations (Ref. 52); dot-dashed curve; momentum density for $1p$ simple harmonic oscillator (SHO) wave function (Ref. 50). For $q > 660$ MeV/$c$, all curves have been multiplied by 1000.

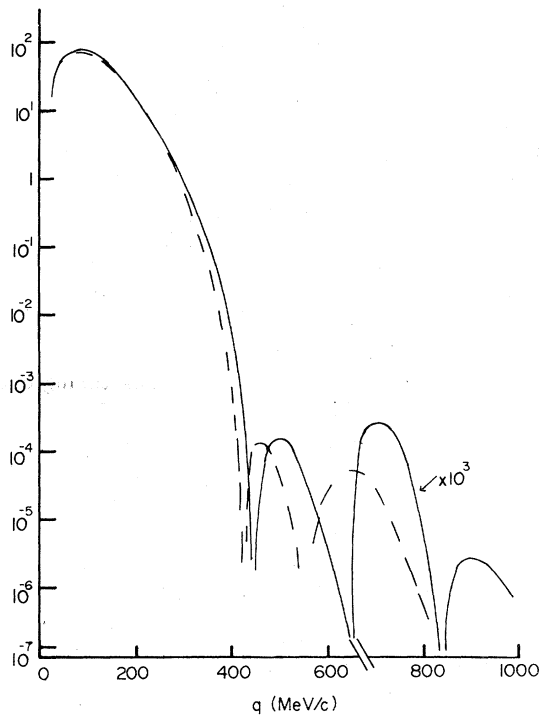


FIG. 2. Single-particle momentum density $\Omega(q)$, in $(\mathrm{GeV}/c)^{-3}$, vs momentum $q$ in MeV/$c$, for $1p_{1/2}$ protons in $^{16}$O. Solid curve: Elton-Swift $1p_{1/2}$ wave function for $^{16}$O; dashed curve: Fourier transform of Negele density-dependent Hartree-Fock wave function for $^{16}$O. For $q > 660$ MeV/$c$ the Elton-Swift curve has been multiplied by 1000.

densities obtained through such wave functions give reasonable agreement with electron scattering data for momentum transfers below 600 MeV/$c$[56]; the momentum density drops off extremely rapidly for momenta above 500 MeV/$c$. The solid curve in Figs. 1 and 2 is the momentum density for an Elton-Swift $1p_{1/2}$ wave function for $^{16}$O; Elton and Swift[57] found a Woods-Saxon potential which would produce $^{16}$O single-particle wave functions with binding energies and electron scattering cross sections which reproduced experimental data (for $^{16}$O it fitted elastic electron scattering data at 420 MeV). The resulting momentum wave function has zeros at approximately 450, 650, and 850 MeV/$c$ (for momenta greater than 650 MeV/$c$ this wave function has been multiplied by $10^3$). The dashed curve in Fig. 2 is the Fourier transform of a $1p$-shell wave function for protons in $^{16}$O due to Negele, from his density-dependent Hartree-Fock calculations.[58] Negele's wave functions have considerably larger high-momentum components (for moments greater than 600 MeV/$c$) than the Elton-Swift, since Negele's calculations include a more realistic inclusion of the short-range components of the two-nucleon interaction.

The discrepancy between the Elton-Swift and Negele wave functions at high momentum gives a measure of the uncertainty in the single-particle high-momentum components for two calculations which are both fitted to electron scattering data. For the $(\gamma, p)$ reaction on $^{16}$O at a photon lab energy of 350 MeV and proton scattering angle (relative to the incident photon direction) of 120°, the momentum difference $q$ is approximately 1 GeV/$c$, where the single-particle wave functions are not well determined from other experiments. For simplicity in our calculations we have used an oscillator expansion fit to the Negele wave functions in terms of the lowest eight $p$-wave harmonic oscillator functions. The momentum distribution resulting from this expansion is plotted as the dashed curve in Fig. 1; in comparison with the exact wave function as plotted in Fig. 2, we see that for momenta above 700 MeV/$c$ the oscillator expansion does not contain sufficient large-momentum components.

## III. EFFECTS OF NUCLEON DISTORTION

### A. Approximating the nucleon distorted-wave function

In this section we will discuss an approximate treatment of the nucleon-nucleus scattering wave function which will enable us to estimate the effects of distortion of the outgoing nucleon in both the direct knock-out amplitude and in the isobar amplitude. As we are primarily interested in the photonuclear reaction for photon energies of 100 MeV and upwards, we could use nucleon distorted waves obtained either from optical potentials or from the WKB approximation. Lee and McManus[59] have shown that, for the inelastic scattering cross sections of protons from $^{12}$C at 156 MeV incident energy, WKB and DWIA calculations using the same potentials produced extremely similar results, so that we might expect both methods to produce comparable wave functions at these energies. However, some objections to WKB results have been raised by Jackson and collaborators[60]; a discussion of the merits and drawbacks of the WKB approximation for nuclear reactions is given by Austern.[61] If we use the WKB approximation to describe the wave functions, we would have

$$\chi_{\vec{p}}^{(+)}(\vec{r}) = \exp\left(i\vec{p}\cdot\vec{r} - \frac{ip}{2E_N}\int_{-\infty}^{z}[W_1(b,z') + W_2(b,z')\vec{\sigma}\cdot\vec{b}\times\vec{p}]\,dz'\right), \tag{3.1}$$

where $p$ and $E_N$ are the nucleon-nucleus relative momentum and energy, and $W_1$ and $W_2$ are the central and spin-orbit potentials, respectively. In Eq. (3.1), $b$ is the impact parameter defined by $\vec{r} = (\vec{b}, z)$. From Eq. (3.1) (neglecting the spin-orbit contribution for the present) we see that the real part of $W_1$ contributes to the phase of the exponential, while the imaginary part diminishes the magnitude of $\chi^{(+)}$ due to the loss of flux into other reaction channels. As the energy increases, the real part of the optical potential decreases in magnitude, so that the effect of this term can be expected to decrease in importance. For this reason (and because of its simplicity in calculations) we have approximated the distorted nucleon wave as a "modified plane wave"

$$\chi_{\vec{p}}^{(+)}(r) = \sqrt{\xi}\, e^{i\vec{p}'\cdot\vec{r}}. \tag{3.2}$$

In Eq. (3.2), $\vec{p}$ is the asymptotic nucleon momentum, $\sqrt{\xi}$ is the magnitude of the nucleon wave function in the nuclear interior, and $\vec{p}'$ is the effective local momentum of the nucleon under the influence of the nuclear force. We include both a real and a (small) imaginary part for $\vec{p}'$; the real part represents the shift in the real wave number due to the real part of the nuclear potential. The influence of the absorption is seen both in the reduction factor $\sqrt{\xi}$ and in the imaginary part of $\vec{p}'$; since most of the effect of the absorption is included in $\xi$, we find that the imaginary part of $p'$ is quite small. We choose the directions as $\vec{p}' \equiv \hat{p}$.

For lower-energy proton-nucleus scattering, McCarthy and collaborators[49] made detailed studies of approximations to nucleon distorted-wave functions. They showed that the distorted proton wave function could be accurately described as a sum of two terms: a modified plane-wave piece plus a "focus" term. The latter piece resulted from the focusing of the nucleon wave by the nucleus. This focusing effect produced a pronounced maximum in the magnitude of the proton wave function near the back of the nucleus (i.e., the side opposite the direction of the incident proton beam). The importance of a focusing effect would rule out a modified plane-wave description such as that of Eq. (3.2). In Fig. 3 we show the magnitude of the wave function for protons incident on $^{13}$C at energy 20 MeV. The wave function has been generated from a Woods-Saxon optical potential,[62] and the diagram shown contains slices taken at 15° intervals from 0–180°. The beam in this case is incident from the right, and the dashed line represents the half-density radius of the optical potential which generated the wave function. The focus at the back of the nucleus is very prominent, and it greatly influences the proton wave function inside as well as outside the nuclear radius. In Fig. 4 the contours of constant phase are plotted for this wave function. Again the influence of the focus

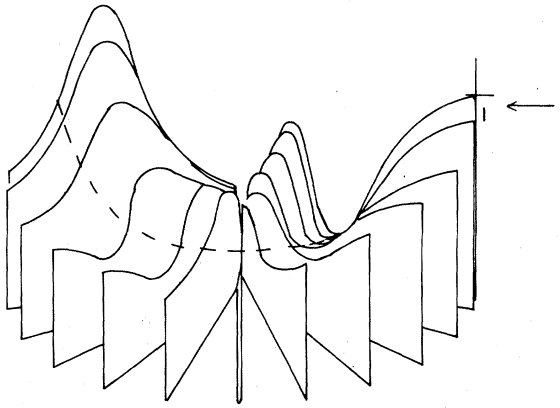


FIG. 3. Magnitude of optical model wave function for 20 MeV protons on $^{13}$C with parameters $V_0 = 50$ MeV, $W = 6$ MeV, $r_0 = 1.2$ fm, and $a = 0.55$ fm. The beam is incident from the right, and slices are shown every 15°. The dashed curve gives the half-density radius of the optical potential which produced this wave function. The importance of the focus is evident in the rapid variation of the magnitude across the nuclear region. The scale at right shows the magnitude of the wave function (relative to plane wave).

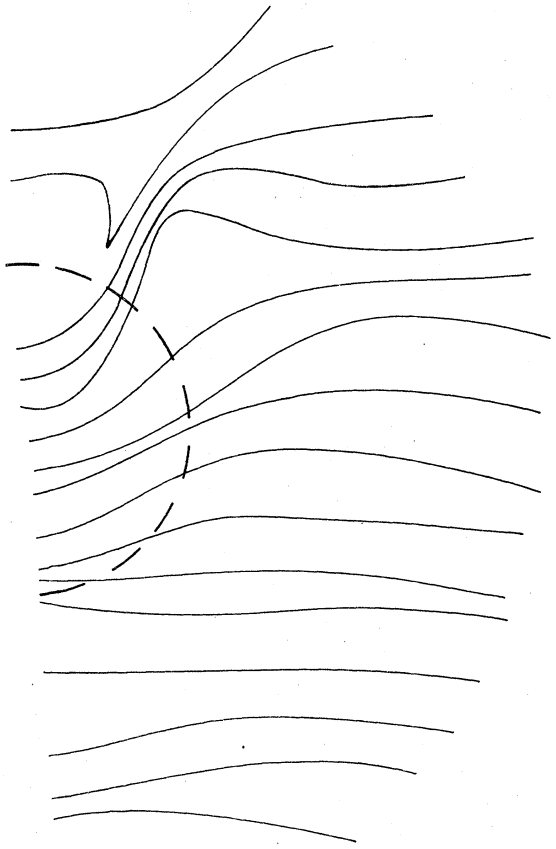

FIG. 4. Lines of constant phase for the optical model wave function for 20 MeV protons on $^{13}C$, with parameters listed in Fig. 3. The dashed line indicates the half-density radius of the optical potential. The beam is incident from the bottom in this figure.

is apparent, since a modified plane-wave approximation would predict straight lines normal to the incident beam direction for the phase contours.

As the proton energy increases, the "focus" term gradually diminishes in magnitude, and a modified plane-wave description gives a rather good fit to the actual distorted wave. In Figs. 5 and 6 are shown magnitude and phase diagrams for the wave function describing 156 MeV protons scattering from $^{12}C$, using an optical potential of Satchler and Haybron.[63] In Fig. 5 we plot the magnitude of the non-spin-flip part of the proton wave function; again the proton is incident from the right, and the magnitude of the wave function can be seen to change smoothly over the nuclear volume. Ths phase contours for this wave function, plotted in Fig. 6, are rather close to straight lines, and suggest that the modified plane-wave approximation might provide an accurate description of the distorted wave at these energies.

From optical potential parameters describing

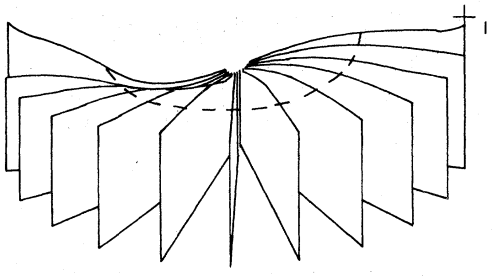

FIG. 5. Magnitude of non-spin-flip part of the optical potential wave function for 156 MeV protons on $^{12}C$ from the optical potential of Satchler and Haybron, Ref. 55. Notation is the same as for Fig. 3; in this case, the "focus" has essentially disappeared.

medium-energy proton-nucleus scattering, we constructed distorted proton wave functions and fitted the non-spin-flip amplitudes to the plane-wave form

$$\chi_{\vec{p}}^{(+)}(\vec{x}) = \sqrt{\zeta}\exp(i\vec{p}'\cdot\vec{r}),$$

where

$$p' \equiv [p^2 + 2\mu(\overline{V} + i\overline{W})]^{1/2} \tag{3.3}$$

and $\hat{p}' = \hat{p}$. In Eq. (3.3), $\mu$ is the $p$-nucleus reduced mass, and $\overline{V}, \overline{W}$, and $\zeta$ were real parameters which were varied to minimize the difference between $\chi_{\vec{p}}$ and the actual distorted wave. As we were interested in the wave function in the vicinity of the nucleus, we fit $\chi_{\vec{p}}(\vec{r})$ and the wave function for $r \leq R$ where $R$ was the half-density radius of the Woods-Saxon optical potential. We performed this analysis for optical potentials fitted to $p + {}^{12}C$ scattering, for which optical potentials have been generated for reactions up to 1 GeV incident en-

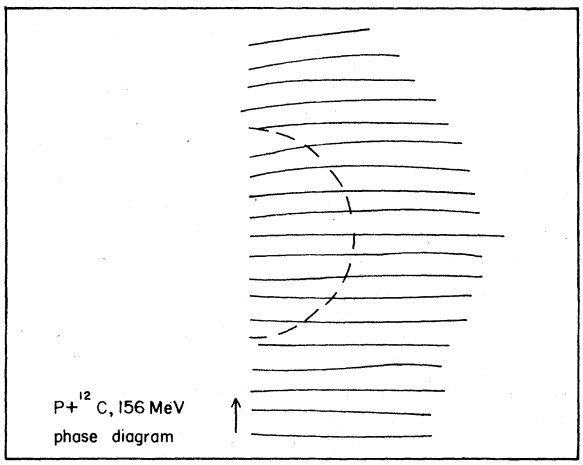


FIG. 6. Lines of constant phase for the non-spin-flip part of the optical model wave function for 156 MeV protons on $^{12}C$. The phase contours are well approximated by straight lines at this energy.

TABLE II. Effective real and imaginary potentials $\bar{V}$ and $\bar{W}$, and magnitude $\zeta$ obtained by fitting non-spin-flip parts of $p+{}^{12}$C scattering wave functions generated from optical potentials. $\bar{V}$, $\bar{W}$, and $\zeta$ are obtained by minimizing the difference between the modified plane-wave parametrization of Eq. (3.3) and the optical-potential wave functions. Also tabulated are the approximate values of Passatore's tabulation of nucleon optical potentials, real and imaginary parts $V_p$ and $W_p$, respectively.

| Proton energy (MeV) | $\bar{V}$ | $\bar{W}$ | $\zeta$ | $V_p$ | $W_p$ |
|---|---|---|---|---|---|
| 75 | 13.5 | −2.0 | 0.47 | 35.0 | 11.3 |
| 100 | 13.0 | 1.4 | 0.53 | 30.1 | 12.6 |
| 156 | 2.9 | 9.1 | 0.55 | 20.0 | 15.5 |
| 182 | −0.34 | 9.6 | 0.55 | 15.7 | 16.8 |

ergy.[64] The parameters $\zeta$, $\bar{V}$, and $\bar{W}$ generated from such a fit are given in Table II. Although there is some scatter in the results, there is clearly a trend towards increasing values of $\zeta$ and $\bar{W}$ and decreasing values of $\bar{V}$ with increasing proton energy. For comparison, we list the real and imaginary potential well depths as estimated by Passatore from a study of phenomenological optical potential fits.[65-67] We should emphasize that Passatore is fitting the central depth of the potential, whereas we have fitted the wave functions themselves; so that a direct comparison of the two numbers may not be reasonable.[68] However, our results certainly confirm the trend found by Passatore for decreasing $V$ and increasing $W$ with energy.

In order to extrapolate between energies, we use formulas for $\zeta$, $\bar{V}$, and $\bar{W}$

$$\zeta = \zeta_0 + \zeta_1 \ln E(\mathrm{MeV}),$$
$$\bar{V} = -V_0\{1 - a_1 \tanh[a_2 E(\mathrm{MeV})]\}, \qquad (3.4)$$
$$\bar{W} = W_0[1 + bE(\mathrm{MeV})].$$

The values of the parameters which best fit $\zeta$, $\bar{V}$, and $\bar{W}$ over the energy region of interest are listed in Table III. In addition to the parameters obtained from fitting the wave functions, we list in Table III values of parameters which give a reasonable fit to the real and imaginary optical potential well depths compiled by Passatore for energies between 20–500 MeV.

TABLE III. Parameters for Eq. (3.4) which best reproduce the energy dependence of modified plane-wave fits to proton scattering wave functions from $^{12}$C. These parameters were then used to estimate distorted-wave calculations for photonuclear reactions. For comparison, we list those parameters which reproduce the energy dependence of Passatore's potentials.

| $\zeta_0$ | $\zeta_1$ | $V_0$ | $a_1$ | $a_2$ | $W_0$ | $b$ |
|---|---|---|---|---|---|---|
| 0.26 | 0.058 | 27.0 | 2.68 | 0.0023 | −12.33 | 0.14 |
| ••• | ••• | 50.6 | 1.35 | 0.0031 | 7.46 | 0.051 |

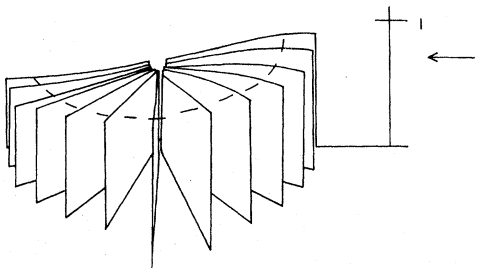

FIG. 7. Modified plane-wave approximation to the magnitude of the optical model wave function of Fig. 5 using the parameters from Table III. The approximate wave function is plotted from 0–4 fm.

With such a parametrization for the distorted-wave function, we are able to reproduce rather accurately the non-spin-flip part of the proton wave function over the region of the nucleus. In Fig. 7 we plot the approximate wave function using the parameters of Table III for protons on $^{12}$C at 156 MeV; this wave function can be compared with that of Fig. 5.

In our calculations we have neglected the spin-flip part of the nucleon-nucleus wave function. In calculating the wave functions from optical potentials we found that the spin-flip term was generally considerably smaller in magnitude than the non-spin-flip term. In Fig. 8 we plot the magnitude of the spin-flip amplitude for $p+{}^{12}$C scattering at 156 MeV. Whereas the non-spin-flip amplitude has magnitude approximately 0.75 over the nuclear region, the spin-flip amplitude is never greater than 0.15. As a result, we have not included the spin-flip part of the nucleon distortion, although we expect the importance of this term to increase at higher energies where the spin-orbit strength becomes appreciable compared with the central part of the optical potential.

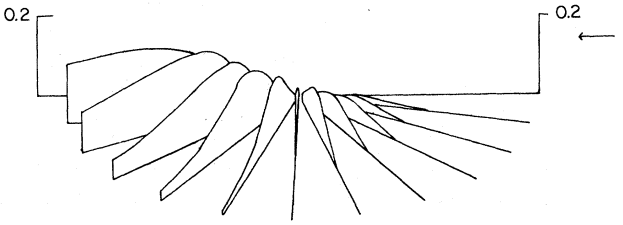


FIG. 8. Magnitude of the spin-flip part of the optical model wave function for 156 MeV protons on $^{12}$C using the parameters of Ref. 55. Note the difference in scale between the magnitude of this amplitude and that of Fig. 5.

The wave functions we have constructed can reproduce rather well the nucleon distorted waves generated from phenomenological optical potentials. They are simple to use and can be included in our calculation of the isobar amplitude with essentially no further increase in the complexity of our numerical calculations. For proton energies above about 70 MeV this approximation is rather accurate; however, with decreasing proton energies the "focusing" term which we previously discussed becomes more and more important and the quality of our fits to distorted-wave functions decreases markedly. As our primary interest is to compare, and evaluate, direct knock-out and isobar amplitudes for photon energies above about 100 MeV, we find this approximation adequate for our purposes; at low energies the modified plane-wave parametrization of Eq. (3.3) does not adequately describe the proton distorted waves.

### B. DWIA calculation of the $(\gamma, p)$ reaction

Using the distorted waves described in Sec. III A, we can straightforwardly calculate the DWIA $(\gamma, p)$ cross sections. In terms of the nucleon momentum in the laboratory frame $\vec{k}_N$, the proton-nucleus relative momentum is given by

$$\vec{p} = \vec{k}_N - \frac{1}{A}\vec{k}_\gamma ;$$

in terms of the (complex) quantity $\alpha \equiv p'/p$, where $p'$ is obtained from Eq. (3.3), we obtain

$$\frac{d\sigma^{\mathrm{DWIA}}}{d\Omega_{\mathrm{lab}}} = \frac{\pi e^2 \zeta}{2}\frac{{k_N}^2}{k_\gamma}\frac{dk_N}{dE_f}\frac{1}{(2\pi)^3}\frac{(2j+1)}{(2l+1)} \times \sum_m |\varphi_{nljm}(\vec{q}')|^2 \left(\frac{|\vec{p}'|^2}{M^2}\sin^2\theta + \frac{{k_\gamma}^2}{2M^2}\mu_p{}^2\right). \tag{3.5}$$

In Eq. (3.5)

$$\vec{q}' = \alpha\vec{k}_N - \left(1 + \frac{\alpha - 1}{A}\right)\vec{k}_\gamma ,$$
$$\vec{p}' \equiv \alpha\left(\vec{k}_N - \frac{1}{A}\vec{k}_\gamma\right). \tag{3.6}$$

With the modified plane waves, the cross section is again proportional to the square of the single-particle momentum wave function (although the "effective momentum" $q'$ in our calculation has a slight dependence on the photon energy, as well as a small imaginary part). We can again define a "momentum density" by dividing the cross section by a kinematic factor in analogy with the derivation of Eq. (2.11); in Fig. 9 we plot this momentum density vs the effective momentum $|\vec{q}'|$ for the reaction $^{16}O(\gamma, p_0)^{15}N$. The curve is the result from the oscillator expansion of Negele's wave functions,[58] and the data points are the results of Matthews *et al.*[41,43] (closed circles) from the Bates linac, and the Glasgow measurements of Findlay and Owens[35] (open circles).

The data and the Negele momentum distribution exhibit two very striking features. First, the "scaling" behavior predicted by DWIA seems to be very well satisfied, in that experimental results obtained at different photon energies and scattering angles seem to lie on a universal curve when kinematic factors are extracted and the data is plotted against the magnitude of the effective momentum (at least, this is true for momenta below 500 MeV/$c$). Second, the data agrees extremely well with the Negele single-particle momentum density for momenta below 400 MeV/$c$. This has been emphasized by Findlay *et al.*[38,40,42,69]

If one used a PWIA calculation and compared the lower-energy data ($|q| \lesssim 400$ MeV/$c$) with the theoretical momentum distribution, the agreement would not be nearly as good as for the distorted-wave results. One additional argument supporting this analysis is that for $^{12}C$ targets the $(\gamma, p)$ experiments can be compared with $(e, e'p)$ knock-out reactions.[70] The highest-momentum transfers reached so far in $(e, e'p)$ measurements correspond to momenta probed in the low-energy $(\gamma, p)$ reactions; when analyzed in a consistent manner, the momentum densities from the two experiments are in excellent agreement with each other and are in good agreement with the theoretical momentum density.[39] It would appear that at least the lower-energy photonuclear data shows convincing evidence of dominance by direct knock-out processes, and that the single-particle momentum density can in fact be extracted from experimental cross sections.

However, there are two corrections to this analysis which might alter these results considerably. The first is the possible importance of nucleon charge-exchange processes following the photon absorption. As we have mentioned previously, the DWIA analysis presented here would predict very small $(\gamma, n)$ cross sections for photon energies below 100 MeV, whereas experimental measurements of $(\gamma, n)$ reactions[34] obtain cross sections which are within a factor of 2 of the $(\gamma, p)$ results. If the charge-exchange process were important, then we could obtain significant numbers of neutrons from a $(\gamma, p)$ reaction followed by $(p, n)$. Calculations done by Cotanch[71] suggest that such an amplitude could be significant in the region below 100 MeV. A similar result also occurs in the work of Gari, Hebach *et al.*[72,73] who use a continuum shell model containing a charge-changing two-particle residual interaction. Such an interaction gives rise to suitably large $(\gamma, n)$ cross sections

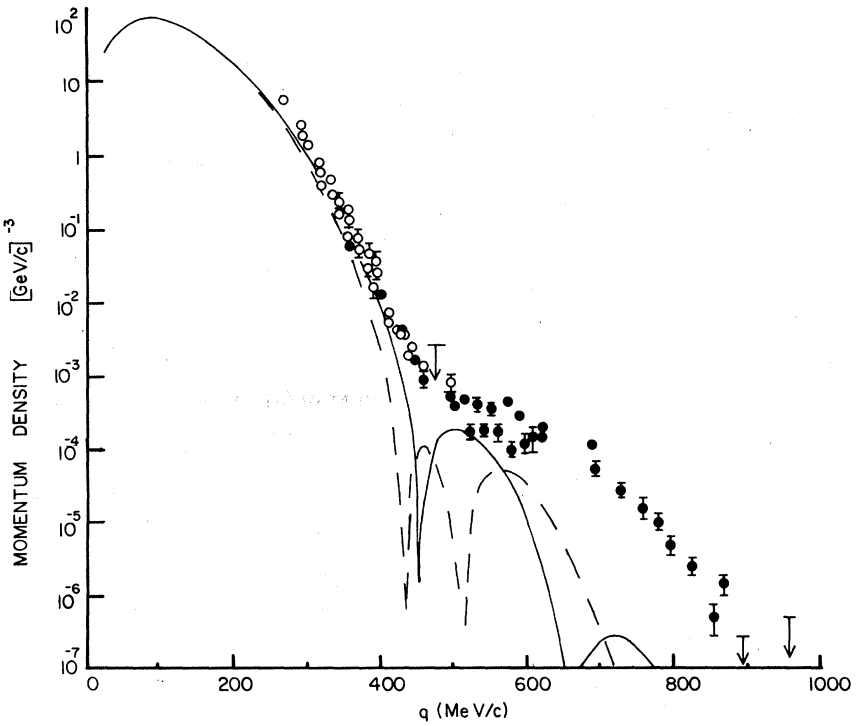


FIG. 9. Momentum density, in $(\mathrm{GeV}/c)^{-3}$ vs effective momentum $|q'|$ in MeV/$c$ for the reaction $^{16}\mathrm{O}(\gamma,p_0)^{15}\mathrm{N}$. Solid curve: DWIA calculation using Elton-Swift bound-state wave function, and a modified plane wave for proton scattered wave with parameters given in Table III. Dashed curve: DWIA calculation using the oscillator expansion of Negele's density-dependent Hartree-Fock wave function, and a modified plane wave for the proton scattering wave function with parameters given in Table III. Data points are Glasgow measurements of Findlay and Owens, Refs. 38 and 40, open circles; and closed circles are Bates Linac results of Matthews *et al.* (Refs. 41 and 43).

for energies below 140 MeV.[8] If the charge-exchange process is important, however, the inclusion of this in the $(\gamma,p)$ amplitude may cause considerable change in the predictions of the "momentum density."

A second question regards the orthogonality of initial and final-state wave functions. Noble[54] has recently shown that, provided one generates both the initial bound state and final scattering state wave functions from the same real (and energy-independent) potential, one can show that both the convective and magnetic moment amplitudes calculated using these orthogonal wave functions will be suppressed relative to a plane-wave result. Also, the magnetic moment term will be suppressed to a much greater degree than will the convective term; the suppression factor for the magnetic term (relative to plane wave) is predicted by Noble to be about $(k_\gamma/k_N)^2$. Such results had been obtained in a calculation by Fink *et al.*,[75] who found the magnetic amplitude to be greatly suppressed when they used the same real central Woods-Saxon potential to generate bound and scattering wave functions for a $(\gamma,p)$ calculation. We have not included orthogonality corrections in our calculations. We are primarily interested in the region of photon energy from 100–400 MeV; in this region, the *effective* proton nucleus interaction is known to have strong absorption due to competing nuclear channels and to be significantly weaker than the binding potential for the same proton. Although use of an energy-independent real central potential allows one to guarantee orthogonality of initial and final wave functions it provides an unrealistic description of the distortion of the outgoing proton. A realistic calculation requires attention to both orthogonality and the many-channel nature of the final state; Noble has outlined a method for such a calculation but it is not clear what effects this would have on our present calculation of the magnetic moment amplitude.

## IV. ISOBAR AMPLITUDE IN $(\gamma,N)$ REACTIONS

In addition to the direct knock-out reactions, we expect to see significant contributions to the nuclear photoeffect from exchange-current processes where a photon shares the transferred momentum with two or more interacting nucleons. We expect the exchange-current diagrams which proceed via pion exchange to be the dominant exchange-cur-

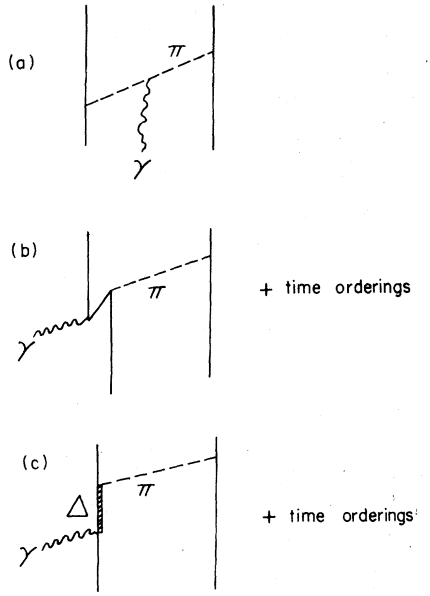


FIG. 10. Lowest-order one-pion range exchange currents which contribute to photonuclear knock-out reactions. (a) the "pionic" current, where a photon attaches to an exchanged pion; (b) "pair" current, where a photon connects with a nucleon-antinucleon line; (c) "isobar" current, where a $\gamma N\Delta$ vertex is accompanied by isobar decay to virtual pion plus nucleon. Diagrams (a)–(c) must be summed over all time orderings which occur.

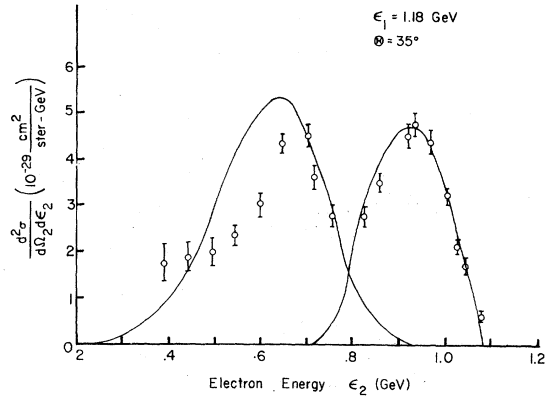


FIG. 11. Inelastic electron scattering on tungsten. Differential cross section $d^2\sigma/d\Omega_2 d\epsilon_2$, in $10^{-29}$ cm$^2$/sr-GeV vs scattered electron energy $\epsilon_2$ in GeV; $\epsilon_2$ and $\Omega_2$ are the energy and solid angle for the scattered electron. Data points are those of Titov *et al.*, Ref. 45, for incident electron energy 1.18 GeV and scattering angle 35°; theoretical curves are from a Fermi-gas calculation due to Moniz, Ref. 46, with parameters $k_F = 268$ MeV/$c$ and $\bar{\epsilon} = 42$ MeV.

rent processes at lower energies since pion exchange provides the longest-range piece of the two nucleon strong interaction. In Fig. 10 we show some of the lowest-order pionic exchange-current diagrams which contribute to $(\gamma, N)$ reactions. The "pionic" and "pair" current graphs of Fig. 10(a) and 10(b), respectively, will contribute primarily to electric exchange-current terms, whereas the "isobar current" term of Fig. 10(c) will contribute to the magnetic exchange currents. For photon energies up to about 400 MeV we would expect the isobar current to provide the dominant magnetic exchange-current term.

In other electromagnetic reactions, the effects of isobar photoexcitation can be quite prominent. For example, in quasielastic electron scattering where no hadrons are observed in the final state, the nuclear response function shows the effect of isobar excitation quite clearly. Figure 11 shows the cross section $d^2\sigma/d\Omega_2 d\epsilon_2$ ($\Omega_2$ and $\epsilon_2$ being the solid angle and energy for the outgoing electron) for 1.18 GeV incident electrons on tungsten and a scattering angle of 35°, versus the energy of the scattered electron. The data is that of Titov *et al.*[45] and the theoretical calculation is due to Moniz.[46] The peak at higher $\epsilon_2$ is due to single nucleon knock-out (in a Fermi-gas nuclear model) and the lower-energy peak is the result of isobar photoexcitation in the same nuclear model. The data show the two peaks very prominently and the isobar and nucleon knockout peaks are clearly separated. In such an "inclusive" reaction, the cross sections depend primarily upon the isobar-production amplitude and the "effective mass" of the isobar in the nuclear medium. As we will show, the nuclear form factors become very important in determining $(\gamma, p)$ reactions to specific nuclear final states, and it is interesting to see whether the sharp peak seen in quasieleastic electron scattering survives in measurements of the nuclear photoeffect to discrete nuclear states.

In I, we considered the contribution of the isobar $\Delta(1232)$ excitation to the reaction $^{16}O(\gamma, p_0)^{15}N$ (the proton subscript referring to the ground state of the residual nucleus). At that time, preliminary data for this reaction had been obtained at the Bates linac. Our calculation showed that isobar photoexcitation should be large in the photon energy region 100–400 MeV, and that our results reproduced the magnitude and at least the qualitative behavior of the observed cross sections. Since that time, a considerable amount of additional experimental data have been acquired for this same reaction,[41,43] and we have extended our previous work to include many features which had not been included in our original letter. In this section we will outline the isobar contribution to $(\gamma, N)$ reactions and present some results, and in Sec. V we will extend the model outlined in this section and discuss at some length the sensitivity of the amplitudes to our choices for several of the param-

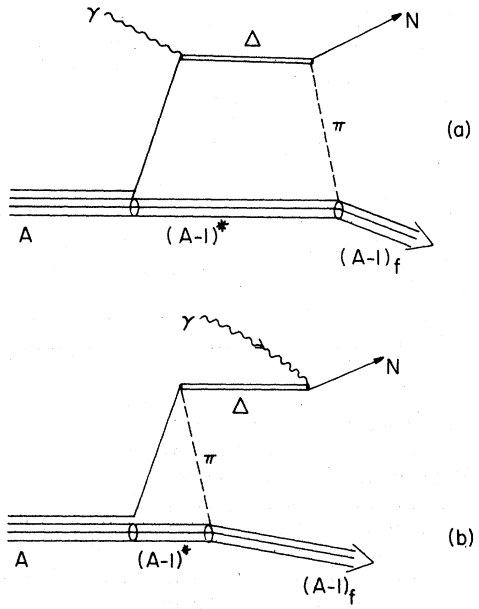


FIG. 12. Diagrammatic representation of isobar contributions to the nuclear photoeffect. (a) The $\Delta(1232)$ is created by photoexcitation of a nucleon, propagates, and then decays to a nucleon plus pion, the pion being absorbed by the residual nucleus. (b) The isobar is created in the nucleus and is then converted to a nucleon by absorbing the incident photon.

eters in this model.

In Fig. 12 we give a diagrammatic representation of the isobar contributions we have calculated for $(\gamma, N)$ reactions. In Fig. 12(a) the $\Delta(1232)$, a $J = \frac{3}{2}$, $T = \frac{3}{2}$ baryon with mass 1232 MeV and free width approximately 115 MeV, is created by photoexcitation of a nucleon. The resulting intermediate state contains a virtual isobar and a one-hole state of the target nucleus. The isobar then decays into a pion plus a nucleon, the pion being absorbed by the residual nucleus to produce the observed final nuclear states. In Fig. 12(b) the photon is absorbed subsequent to the isobar formation, deexciting the $\Delta$ to the final nucleon $N$.

The amplitudes which we use in evaluating this process are just the off-shell extension of the pion photoproduction amplitude $\gamma + N \rightarrow N + \pi$, since we neglect the isobar-nucleus interaction in our calculation (that is, we do not include isobar self-energy terms). This amplitude has been studied in detail since it dominates low-energy pion photoproduction,[76,77] and we use it to fix the coupling constants and matrix elements for the $\gamma N\Delta$ and $\Delta N\pi$ vertices. In calculating the isobar contribution to this process, we may write the amplitudes in terms of isobar creation and decay matrix elements

$$M_{fi} = \sum_{\substack{\text{intermediate}\\ \text{states}}} \langle \chi_N^{(-)} \psi_f^{A-1} | H_{\text{decay}} | \psi_\Delta \psi_{\text{int}}^{A-1} \rangle \frac{1}{E - (p_\Delta{}^2/2M_\Delta + M_\Delta - i\Gamma/2) - E_{\text{int}}} \langle \psi_\Delta \psi_{\text{int}}^{A-1} | H_{\text{prod}} | \psi_i^A \rangle$$
$$+ \langle \chi_N^{(-)} \psi_f^{A-1} | H_{\text{prod}}^\dagger | \psi_\Delta \psi_{\text{int}}^{A-1} \rangle \frac{1}{E - E_\gamma - (p_\Delta{}^2/2M_\Delta + M_\Delta - i\Gamma/2) - E_{\text{int}}} \langle \psi_\Delta \psi_{\text{int}}^{A-1} | H_{\text{decay}}^\dagger | \psi_i^A \rangle . \quad (4.1)$$

In Eq. (4.1), $|\psi_i^A\rangle$ is the initial $A$-particle target nucleus, and the final state is the product of a nucleon-nucleus relative wave function $\chi_N^{(-)}$ ($N$ refers to the final ejected particle, either neutron or proton) and the $(A-1)$-particle residual nucleus in state $f$. We will restrict our considerations (for the time being) to transitions where the final state can be written as a one-hole state with respect to the original nucleus, i.e.,

$$|\psi_f^{A-1}\rangle = a_f |\psi_i^A\rangle , \quad (4.2)$$

where $a_f$ represents annihilation of a nucleon with quantum numbers $f$. We will evaluate Eq. (4.1) in the laboratory system, so that $E$ is the total laboratory energy (photon energy $E_\gamma$ plus target rest mass), $M_\Delta$ is the isobar rest mass (1232 MeV), $\Gamma$ is the isobar width in the nuclear medium, and $E_{\text{int}}$ is the total energy (kinetic plus rest mass) of the intermediate state of the residual nucleus. The sum over intermediate states includes integration over the isobar momentum, and a sum over all spin and isospin states of the isobar as well as over all quantum numbers of the contributing nuclear states.

In second-quantized form, we can write the required matrix elements as

$$\hat{H}_{\text{prod}} = \sum_{i,k} b_i^\dagger a_k \langle i | M_{\gamma N\Delta} | k \rangle ,$$
$$\hat{H}_{\text{decay}} = \sum_{i,j,k,l} a_i^\dagger a_j^\dagger b_k a_l \langle i,j | M_{\Delta N \rightarrow NN} | k,l \rangle . \quad (4.3)$$

In Eq. (4.3), $b^\dagger$ and $b$ are isobar creation and destruction operators, respectively, and $a^\dagger$ and $a$ are the corresponding nucleon operators. In evaluating Eq. (4.1), we restrict our consideration to intermediate nuclear states which can be represented as single-hole states built from the target nucleus,[78] i.e.,

$$|\psi_{\text{int}}^{A-1}(\alpha)\rangle \equiv a_\alpha |\psi_i^A\rangle .$$

Then we can straightforwardly carry out the commutation relations to obtain the full isobar amplitude

$$M_{fi}^{(\Delta)} = \sum_{\alpha,\Delta}\int \frac{d^3p_\Delta}{(2\pi)^3}\Big[ {}_A\langle N,\alpha|M_{\Delta N\to NN}|\Delta,\alpha\rangle \frac{1}{E-(p_\Delta{}^2/2M_\Delta+M_\Delta-i\Gamma/2)-E_\alpha^{A-1}}$$

$$\times\langle\Delta|M_{\Delta N\gamma}|f\rangle - {}_A\langle N,\alpha|M_{\Delta N\to NN}|\Delta,f\rangle \frac{1}{E-(p_\Delta{}^2/2M_\Delta+M_\Delta-i\Gamma/2)-E_\alpha^{A-1}}\langle\Delta|M_{\Delta N\gamma}|\alpha\rangle$$

$$+\langle N|M_{\Delta N\gamma}^\dagger|\Delta\rangle \frac{1}{E-E_\gamma-(p_\Delta{}^2/2M_\Delta+M_\Delta-i\Gamma/2)-E_f^{A-1}}$$

$$\times\langle\Delta,\alpha|M_{\Delta N\to NN}^\dagger|f,\alpha\rangle_A - \langle\alpha|M_{\Delta N\gamma}^\dagger|\Delta\rangle \frac{1}{E-E_\gamma-(p_\Delta{}^2/2M_\Delta+M_\Delta-i\Gamma/2)-E_f^{A-1}}$$

$$\times\langle\Delta,N|M_{\Delta N\to NN}^\dagger|f,\alpha\rangle_A\Big]. \tag{4.4}$$

In Eq. (4.4), the states $\{\alpha\}$ include all single-particle occupied states in the target nucleus [for $^{16}O(\gamma,P_0)^{15}N$, the sum includes protons and neutrons in $1s_{1/2}$, $1p_{1/2}$, and $1p_{3/2}$ orbits]. The subscript $A$ in the $\Delta N\to NN$ amplitudes denotes antisymmetrization with respect to the two-nucleon state. To evaluate the amplitudes shown in Fig. 12, we first assume plane waves for the outgoing nucleon wave function (we will remove this assumption in Sec. V). For the isobar-production vertex we used amplitudes calculated by Thornber[80] for isobar electroproduction. This amplitude could be written in the form

$$\langle\Delta|M_{\Delta N\gamma}^\lambda|\alpha\rangle = ce\mu_p\sqrt{k_\gamma}\exp\left(-\frac{k_\gamma{}^2 b_Q{}^2}{6}\right)$$

$$\times\langle\chi_\Delta|T_0\vec{S}\cdot\vec{\epsilon}^\lambda\varphi_\alpha(\vec{p}_\Delta-\vec{k}_\gamma)|\chi_\alpha\rangle\,. \tag{4.5}$$

In Eq. (4.5), $|\chi_\alpha\rangle$ and $|\chi_\Delta\rangle$ are spin-isospin wave functions for a nucleon (in single-particle state $\alpha$) and isobar, respectively. $\vec{S}$ (and $\vec{T}$) are matrices which connect spin (isospin) states $\frac{1}{2}$ and $\frac{3}{2}$; these operators are defined so as to reproduce the matrix elements obtained from coupling nucleons with isobars.[81] (The matrices $S$ and $T$ are given vector labels since they are associated with a vector index as described in Ref. 81). In Eq. (4.5), $e$ is the proton charge, $\mu_p$ is the proton magnetic moment in nuclear magnetons, $k_\gamma$ is the photon momentum, $b_Q$ is a size parameter for the nucleon wave functions [we used the value $b_Q = 4$ (GeV/$c$)$^{-1}$ obtained by Thornber], and $c$ was a parameter which we varied to reproduce the observed isobar radiative width[44,77]: We used $c = 1.33$. In Eq. (4.5), $\varphi_\alpha(\vec{q})$ is the single-particle momentum wave function for a bound nucleon with quantum numbers $\{\alpha\}$, defined by

$$\varphi_\alpha(\vec{q}) \equiv \int d^3x\, e^{-i\vec{q}\cdot\vec{x}}\psi_\alpha(\vec{x})\,, \tag{4.6}$$

where $\psi_\alpha(\vec{x})$ is the spatial wave function associated with the state $\{\alpha\}$. Thornber derived Eq. (4.5) using a quark model for the baryons in order to calculate isobar electroproduction cross sections. In the Appendix, we reproduce a derivation of her amplitude and show that it is equivalent to Eq. (4.5).

For the isobar decay $\Delta\to N+\pi$, with absorption of the virtual pion by the residual nucleus, we use an amplitude of the form

$$\langle N,\alpha|M_{\Delta N\to NN}|\Delta,\beta\rangle = \frac{-ff^*}{m_\pi{}^2}\langle\chi_N|\vec{S}^\dagger\cdot\vec{q}T_i^\dagger|\chi_\Delta\rangle\frac{1}{|\vec{q}|^2+m_\pi{}^2}$$

$$\times\langle\chi_\alpha|\vec{\sigma}\cdot\vec{q}\tau_i\rho_{\alpha\beta}(\vec{q})|\chi_\beta\rangle\,. \tag{4.7}$$

Equation (4.7) gives the amplitude for a transition from an initial state consisting of an isobar and nucleon bound state with quantum numbers $\{\beta\}$ to an outgoing free nucleon $N$ and single bound state nucleon with quantum numbers $\{\alpha\}$. In Eq. (4.7), $\vec{q}$ is the pion momentum, $\vec{q}\equiv\vec{k}_N-\vec{p}_\Delta$ where $\vec{k}_N$ is the asymptotic laboratory momentum of the outgoing nucleon, and $f$ and $f^*$ are the $NN\pi$ and $\Delta N\pi$ coupling constants, respectively. We have used form factors for the coupling constants which are assumed to have the dipole form

$$f(q) \equiv \left(\frac{\lambda^2-m_\pi{}^2}{\lambda^2+|\vec{q}|^2}\right)^2. \tag{4.8}$$

In Eq. (4.8) we have neglected the fourth component of the pion four-momentum; for the reaction we are interested in $q_0$ would be much less than $|\vec{q}|$, in the kinematic region giving a large contribution to the matrix element. We used $f_0 = 1.009$ and $f_0^* = 2.097$ as typical values for the $NN\pi$ and $\Delta N\pi$ coupling constants, and for the form factors we used values fitted to neutrino reactions which gave $\lambda(NN\pi) = 6.8m_\pi$ and $\lambda(\Delta N\pi) = 6.9m_\pi$.[82,83] The quantity $\rho_{\alpha\beta}(\vec{q})$ is the single-particle transition density for momentum transfer $q$, taken between single-particle states with quantum numbers $\{\alpha\}$

and $\{\beta\}$; $\rho_{\alpha\beta}(\vec{q})$ is defined as

$$\rho_{\alpha\beta}(\vec{q}) \equiv \int d^3x\, \psi^\dagger_\alpha(\vec{x})\psi_\beta(\vec{x})e^{-i\vec{q}\cdot\vec{x}}. \tag{4.9}$$

The isobar contribution to the $(\gamma, N)$ reaction is obtained by inserting the amplitudes from Eqs. (4.5) and (4.7) into Eq. (4.4) and performing the necessary summations. In carrying out these sums, we can make use of the relations satisfied by the matrix $\vec{S}$ (and $\vec{T}$),[81]

$$\sum_M = (S_i^\dagger)^{m,M}(S_j)^{M,m'} \equiv (\delta_{ij} - \tfrac{1}{3}\sigma_i\sigma_j)^{m,m'}; \tag{4.10}$$

in Eq. (4.10), $m$ and $m'$ represent nucleon spin indices, $M$ is the isobar spin index, $i$ and $j$ are vector indices associated with $\vec{S}$. Carrying out the sum over isobar spin and isospin states thus reduces the matrices $\vec{S}$ and $\vec{T}$ to relatively simple operators in the spin-isospin space of the nucleons. With the use of Eq. (4.10), we obtain

$$\begin{aligned}
M_{fi}^{(\Delta)\lambda} = &-\frac{ce\mu_p}{3m_\pi^2}\sqrt{k_\gamma}\exp\left(-\frac{k_\gamma^2 b_Q^2}{6}\right)\sum_\alpha\int\frac{d^3q}{(2\pi)^3}f(q)f^*(q)\\
&\times\Bigg\{\frac{\langle\chi_N|[2\vec{\epsilon}^\lambda\cdot\vec{q}-i\vec{\sigma}\cdot(\vec{q}\times\vec{\epsilon}^\lambda)](\delta_{i0}-\frac{1}{3}\tau_i\tau_0)\varphi_f(\vec{p})|\chi_f\rangle\langle\chi_\alpha|\vec{\sigma}\cdot\vec{q}\tau_i\rho_{\alpha\alpha}(q)|\chi_\alpha\rangle}{(E-E_\Delta-E_\alpha^{A-1})(|\vec{q}|^2+m_\pi^2)}\\
&-\frac{\langle\chi_N|[2\vec{\epsilon}^\lambda\cdot\vec{q}-i\vec{\sigma}\cdot(\vec{q}\times\vec{\epsilon}^\lambda)](\delta_{i0}-\frac{1}{3}\tau_i\tau_0)\varphi_\alpha(\vec{p})|\chi_\alpha\rangle\langle\chi_\alpha|\vec{\sigma}\cdot\vec{q}\tau_i\rho_{\alpha f}(\vec{q})|\chi_f\rangle}{(E-E_\Delta-E_\alpha^{A-1})(|\vec{q}|^2+m_\pi^2)}\\
&+\frac{\langle\chi_N|[2\vec{\epsilon}^\lambda\cdot\vec{q}-i\vec{\sigma}\cdot(\vec{q}\times\vec{\epsilon}^\lambda)](\delta_{0i}-\frac{1}{3}\tau_0\tau_i)\varphi_\alpha(\vec{p})|\chi_\alpha\rangle\langle\chi_\alpha|\vec{\sigma}\cdot\vec{q}\tau_i\rho_{\alpha f}(\vec{q})|\chi_f\rangle}{(E-E_\gamma-E_\Delta-E_f^{A-1})(|\vec{q}|^2+m_\pi^2)}\\
&-\frac{\langle\chi_N|[2\vec{\epsilon}^\lambda\cdot\vec{q}-i\vec{\sigma}\cdot(\vec{q}\times\vec{\epsilon}^\lambda)](\delta_{0i}-\frac{1}{3}\tau_0\tau_i)\varphi_f(\vec{p})|\chi_f\rangle\langle\chi_\alpha|\vec{\sigma}\cdot\vec{q}\tau_i\rho_{\alpha\alpha}(\vec{q})|\chi_\alpha\rangle}{(E-E_\gamma-E_\Delta-E_f^{A-1})(|\vec{q}|^2+m_\pi^2)}\Bigg\}.
\end{aligned} \tag{4.11}$$

In Eq. (4.11), $\vec{p}=\vec{k}_N-\vec{k}_\gamma+\vec{q}$ is the momentum of the nucleon which is struck by the photon, $E_\Delta$ is the isobar energy

$$E_\Delta = \frac{|\vec{p}_\Delta|^2}{2M_\Delta} + M_\Delta - \frac{i\Gamma_\Delta}{2}, \tag{4.12a}$$

where

$$\vec{p}_\Delta \equiv \vec{k}_N + \vec{q}, \tag{4.12b}$$

and $E_\alpha^{A-1}$ is the total energy of the intermediate state, a one-hole state created by removing a nucleon with quantum numbers $\{\alpha\}$ from the target. For the case where the target nucleus is a closed shell with $T=0$, all terms in Eq. (4.11) vanish except for the second term.

The isobar amplitude which we have derived is characteristic of a two-step reaction in that the large momentum difference between the incident photon and outgoing proton is shared by two nucleons. The amplitude of Eq. (4.11) is proportional to a convolution integral involving a single-particle momentum wave function $\varphi(\vec{p})$ and a single-particle transition density matrix $\rho(\vec{q})$, compared to the direct knock-out amplitude where the entire momentum is absorbed by a single nucleon. The important contributions to this matrix element will come from processes where the momentum wave functions are relatively large, and hence rather well known from electron scattering and knock-out reactions; consequently, evaluation of the isobar amplitude requires single-particle wave functions in a region where they are fairly well determined from independent experiments.[84] By examination of the isobar amplitude, we see that at the largest momentum differences (i.e., the largest proton angles $\theta$ for a given photon energy), the isobar amplitude is likely to be most important relative to the direct knock-out amplitude due to the ability to share the large momentum transfer in two successive steps. Also, as the photon incident energy gets to be about 300 MeV (roughly the mass difference between nucleon and isobar), the denominator associated with the isobar propagator will become smallest so that we might expect this to produce a peak in the isobar amplitude for photon energies around 300 MeV. Such a peak would be quite broad due to the large isobar width. Therefore, by examining the form of the isobar amplitude, we expect this term to be important for photon energies roughly in the region 200–400 MeV; at lower photon energies we expect the isobar contribution to be more important (relative to the direct knock-out amplitude) at larger proton angles.

We have calculated the matrix elements of Eq. (4.11) and added them to the direct knock-out PWIA amplitudes of Eq. (2.8). We have numerically performed the integration over $q$ using Gauss quadrature for the angles and Gauss-Hermite points for the magnitude of $q$. For nuclear wave functions we have used both simple harmonic oscillator wave functions[56] for $^{16}$O and the oscillator expansion of Negele's density-dependent Hartree-Fock

wave functions,[58] both of which were discussed in Sec. II. For the single-particle separation energies we used 12.1 MeV for $p$-shell states and 30 MeV for $s$-shell states, and for the calculations discussed in this section we took the isobar width as the free width $\Gamma_\Delta = 115$ MeV. In Figs. 13–15 we plot the laboratory differential cross sections, in nb/sr, vs photon energy at a fixed lab scattering angle, for the reaction $^{16}O(\gamma, p_0)^{15}N$. The results are exhibited at angles 30°, 45°, 90°, and 135°. The solid curve is the theoretical cross section including the contribution from the direct knock-out PWIA term plus the isobar amplitude, using the simple harmonic oscillator wave functions for single-particle wave functions; the dashed curve is the PWIA plus isobar result using Negele's wave functions. For comparison, the dot-dashed curve represents the cross section from the PWIA amplitude only, with Negele's wave functions. At low photon incident energies, the PWIA term dominates, but at higher energies the isobar-production term becomes progressively larger relative to the direct term. At a scattering angle of 45°, the isobar amplitude begins to dominate the one-step term at a photon energy of about 180 MeV; at 90° the isobar amplitude begins to dominate at roughly 125 MeV, and at 135° the isobar amplitude is large at 100 MeV.

The experimental data are plotted for the angles 45°, 90°, and 135°; the open circles are the Glasgow data of Findlay and Owens[40] and the closed circles are the Bates results of Matthews *et al.*[41] together with additional preliminary data from the same group.[43] The isobar reproduces at least qualitatively the behavior observed in the data; our model predicts a cross section which is essentially constant, at 45° scattering angle, for photon energies 200–400 MeV; at 90°, we calculate a cross section which exhibits a "shoulder" between 125–175 MeV and which thereafter falls rather steeply with increasing photon energy; at 135° our cross sections change slope at about 100 MeV but thereafter fall quite rapidly.

These results show the importance of isobar excitation over a wide range of photon energies. The isobar amplitude fits the general features of the data, for photon energies as low as 100 MeV at large angles, up to the highest energies presently studied in these experiments. In the region 200–400 MeV where we expect isobar production to be most prominent (since we can think of the isobar roughly as a resonant excitation of a nucleon with excitation energy 300 MeV and width about 100 MeV), the isobar amplitude predicts cross sections which are in reasonable agreement with experiment, and which are certainly of the correct order of magnitude as the data.

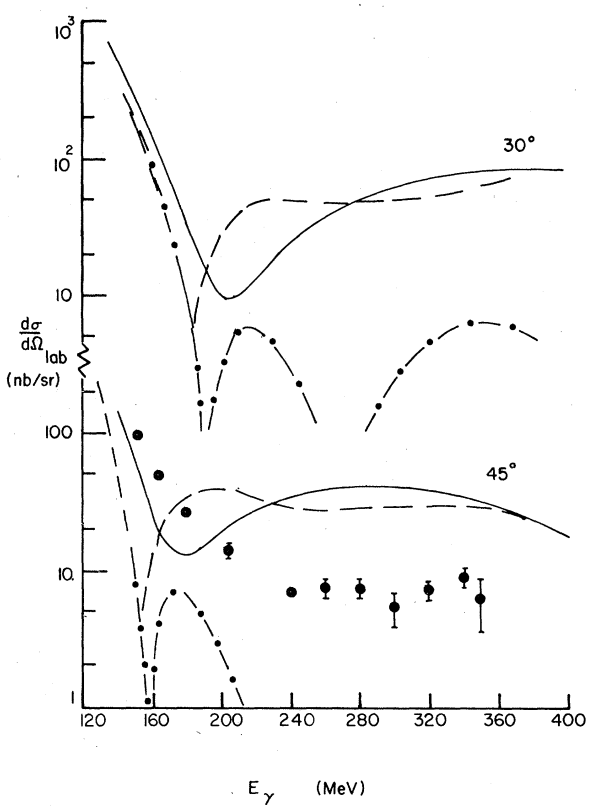


FIG. 13. Laboratory differential cross section $d\sigma/d\Omega$, in nb/sr, vs photon energy $E_\gamma$ in MeV for the reaction $^{16}O(\gamma, p_0)^{15}N$. The results are shown for laboratory proton scattering angles of 30° and 45° relative to the photon direction. In all curves shown here the final-state proton-nucleus interaction has been neglected. Solid curve: theoretical calculation including direct PWIA amplitude plus isobar amplitude using SHO single-particle wave functions; dashed curve: PWIA plus isobar amplitudes using oscillator expansion of Negele wave functions; dot-dashed curve: PWIA amplitude only with Negele single-particle wave functions. Data (at 45°): results of Matthews *et al.*

In the plane-wave calculation shown in this section, we have neglected the interaction of the outgoing nucleon; in addition, we have produced a "zero-parameter" calculation by fixing the values of all parameters in our calculation to independent experimental data. In the following section, we shall first include the final-state interaction of the outgoing nucleon; then we will discuss the sensitivity of our calculation to several of the parameters in our calculation. At that point, we will be able to make a more detailed comparison with the high-quality data which now exist for the $^{16}O(\gamma, p_0)^{15}N$ reaction.

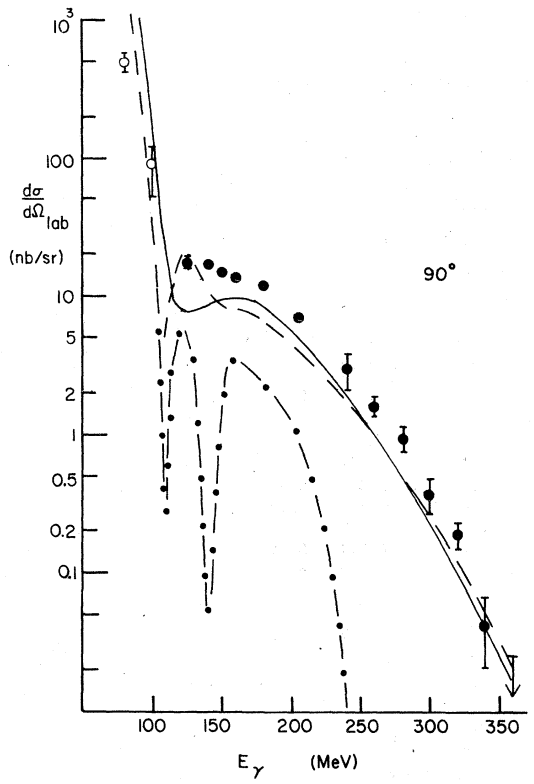


FIG. 14. Lab differential cross sections for $^{16}O(\gamma,p_0)$-$^{15}N$ vs photon energy for scattering angle of 90°. Notation is that of Fig. 13. Data: open circles: results of Findlay and Owens (Ref. 38); closed circles: results of Matthews *et al.*

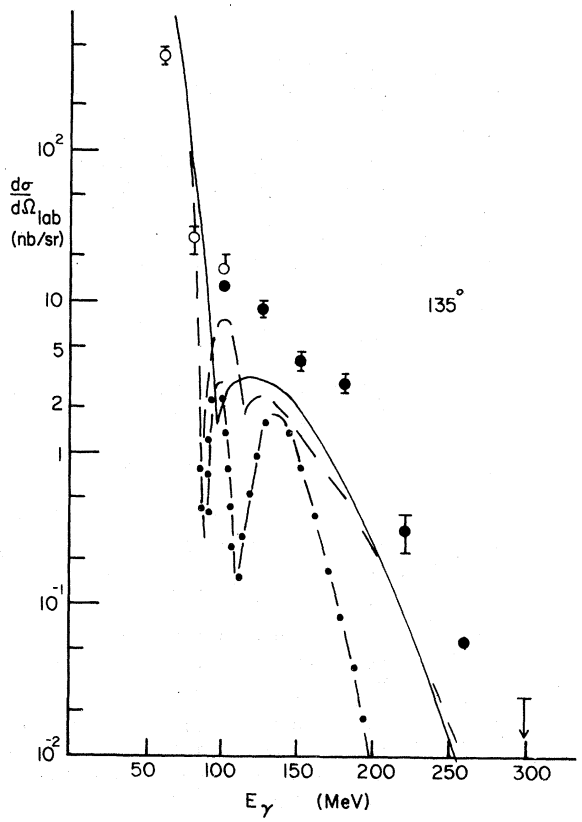


FIG. 15. Lab differential cross sections for $^{16}O(\gamma,p_0)$-$^{15}N$ vs photon energy for scattering angle of 135°. Notation is that of Fig. 13.

## V. FURTHER INVESTIGATION OF THE ISOBAR AMPLITUDE

### A. Inclusion of distorted waves for the outgoing nucleon

In Sec. IV we presented, for the sake of simplicity, a derivation of the isobar contribution to photonuclear reactions which neglected the final-state interaction of the outgoing proton (or neutron). As we are interested in photon energies such that the outgoing nucleon has a relatively large energy (100 MeV or higher), then, as was discussed in detail in Sec. III, a "modified plane-wave" treatment of the nucleon wave function should give good agreement with nucleon wave functions obtained from optical potentials at corresponding energies. The effect of the optical potential is to reduce the flux of the nucleon wave function due to absorptive processes and to shift the effective momentum of the nucleon inside the nucleus due to the real part of the optical potential. It is a straightforward matter to use the approximate wave functions of Sec. III in our isobar photoproduction amplitude; for a given asymptotic nucleon c.m. momentum $\vec{p}$, we use the parameters fitted in that section to calculate the effective (complex) momentum $\vec{p}'$ and overall normalization factor $\sqrt{\zeta}$. The approximate distorted nucleon wave function is then obtained by transforming this wave function to the laboratory reference frame.

In Figs. 16 and 17, we plot the distorted-wave results including the direct and isobar amplitudes versus photon energy for laboratory scattering angles 45° and 90°. In these cases (and in all succeeding figures) we have used the oscillator expansion of Negele's density-dependent Hartree-Fock wave functions for $^{16}O$ bound states. The solid curves are the plane-wave results and the dashed curves are the results of distorted-wave calculations. The deep minima predicted in the plane-wave calculations still survive the distorted-wave calculations but they are shifted to slightly lower photon energies; these minima are not seen in the experimental data and might well be "filled in" in a theoretical calculation if charge-exchange or electric exchange-current effects were included in these calculations. For photon energies great-

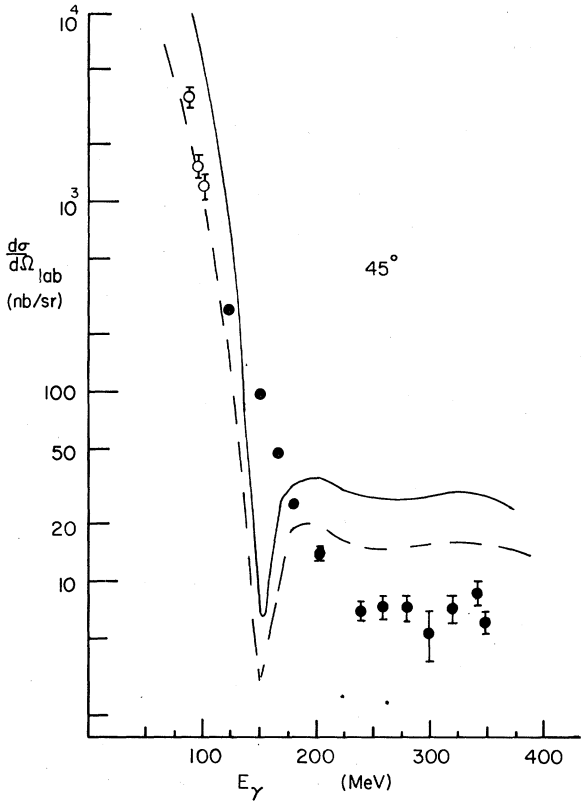


FIG. 16. Laboratory differential cross sections $d\sigma/d\Omega$, in nb/sr vs photon energy $E_\gamma$ (MeV) for $^{16}O(\gamma,p_0)$-$^{15}N$, at proton scattering angle of 45°. Solid curve: direct reaction plus isobar amplitude using plane waves for proton scattering wave function; dashed curve: direct knock-out plus isobar amplitude, with distorted waves represented by modified plane-wave approximation. In this and in all subsequent figures we used the oscillator expansion of Negele's density-dependent Hartree-Fock wave functions. Open circles: results of Findlay *et al*; closed circles: results of Matthews *et al*.

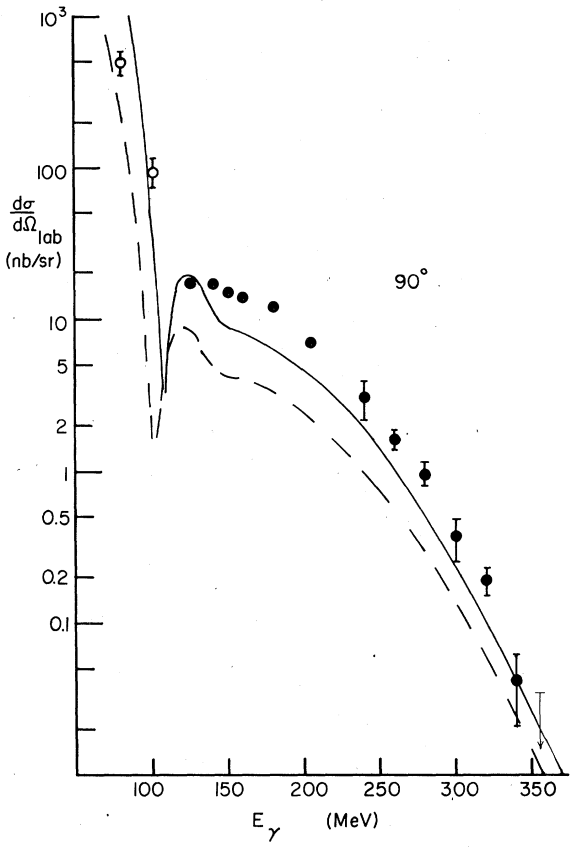


FIG. 17. Lab differential cross sections $d\sigma/d\Omega$ vs photon energy $E_\gamma$ for the reaction $^{16}O(\gamma,p_0)^{15}N$, at proton lab scattering angle of 90°. Notation is that of Fig. 16.

er than about 125 MeV the net result of the distorted-wave calculation is to decrease the plane-wave $(\gamma,p)$ cross sections by roughly a factor of 2. This brings our calculated cross section at 45° into better agreement with the Bates data, but it makes the 90° cross section smaller than the data by a factor of 4 in the energy region from 125–175 MeV.

A more dramatic difference between the plane-wave and distorted-wave results occurs at lower photon energies where the direct reaction dominates in our calculation and where the difference between the "asymptotic" and "effective" nucleon momenta is greater than at higher energies. At photon energy 80 MeV and scattering angle 90°, the distorted-wave amplitude is a factor of 8 smaller than the plane-wave result. For photon energies below 100 MeV, the DWIA amplitudes, using this modified plane-wave approximation to the distorted waves, are in rather good agreement with experimental data, except for the deep minima predicted by the theory but not present in the data. This point has been emphasized by Findlay *et al.*,[38-40] and our calculations obtain similar results. However, we should mention that for photon energies below 100 MeV the modified plane-wave approximation may no longer give an adequate representation of the nucleon distorted-wave function so that our distorted-wave results for low photon energy might not be equivalent to the results from a DWIA calculation using actual wave functions obtained from optical potentials.

The formalism we have outlined can be used to calculate transitions to any nuclei which are one-hole states relative to the target nucleus. At present, experimental studies at medium energies have been limited to the ground state of the residual nucleus (or in a few cases, to a group of low-lying excited states) because of the difficulty of separating transitions to specific excited nuclear

states. However, if such data were available it might provide very useful additional information about the reaction mechanism for the nuclear photoeffect at medium energies. In the plane-wave impulse approximation, the ratio of cross sections leading to two different one-hole states is just equal to the ratio of the single-particle wave functions for the two transitions (to within an overall constant). If the excitation energy for the two states is similar, then the two single-particle wave functions will be evaluated at very nearly the same momentum. Consequently, if PWIA were valid then the measurement of photonuclear cross sections to the ground and certain excited states of the residual nucleus would give a direct comparison of the single-particle momentum components for the states involved.

For example, we consider the reaction $^{16}O(\gamma,p)^{15}N^*$ leading to the 6.32 MeV ($\frac{3}{2}$, –) state of $^{15}N$. This state is well approximated as a $1p_{3/2}$ hole relative to the $^{16}O$ ground state, and we may compare this reaction with the photonuclear reaction to the $^{15}N$ ground state (presumed to be a $1p_{1/2}$ hole relative to $^{16}O$). If we neglect the spin-orbit splitting of the $1p$-shell wave functions, then PWIA would predict that the cross section for $^{16}O(\gamma,p)^{15}N^*$ would be just twice the cross section to the ground state of $^{15}N$ (since there are twice as many $p_{3/2}$ protons as $p_{1/2}$ protons in $^{16}O$). When spin-orbit forces are included, the difference in cross section would just reflect the relative momentum components of the two wave functions. In Fig. 18, we show the momentum distributions $\Omega(q)$ [see Eq. (2.15)] for the $p_{3/2}$ and $p_{1/2}$ proton wave functions in $^{16}O$ using the potential of Elton and Swift.[57] Here, for purposes of comparison, the $p_{3/2}$ momentum distribution has been multiplied by $\frac{1}{2}$ so that in the absence of spin-orbit forces the two distributions would be identical. With this parametrization, the momentum distributions each have zeros which are out of phase with one another; the $p_{3/2}$ wave function has zeroes at about 400 and 600 MeV/$c$ while the first two zeroes of the $p_{1/2}$ wave function occur at 460 and 660 MeV/$c$, respectively. The PWIA cross sections would then reflect these out of phase oscillations.

On the other hand, the isobar amplitude (which involves summation and integration over the nuclear one-hole states) would not be expected to yield the same behavior at all. We have calculated the differential cross section leading to the 6.32 MeV state of $^{15}N$ and compared it with the cross section to the $^{15}N$ ground state. In Fig. 19, we plot the ratio of the ($\frac{3}{2}$ –) cross section to the ($\frac{1}{2}$ –) cross section as a function of incident photon laboratory energy. The solid curve is calculated for proton lab scattering angle of 45° and the dashed curve for 90°. We used distorted waves approximated as described in Sec. III, and we used Negele's wave functions for the proton bound state. Since the bound-state wave functions which we used had no spin-orbit splitting, we would predict a ratio of 2 for the direct term, and at low energies this is what we obtain. At higher energies, where the isobar current begins to dominate, the cross section again becomes close to 2; consequently in this case the isobar current which we have calculated does not change the predictions markedly from that given by the impulse approximation.

Since we are using bound-state wave functions which do not differentiate between the $p_{3/2}$ and $p_{1/2}$ protons, our calculation here can just give a qualitative estimate for the relative cross sections, particularly since Fig. 18 shows large differences between $p_{1/2}$ and $p_{3/2}$ wave functions at large momentum. However, with our choice of wave function and including the isobar amplitude, the *ratio* of the cross sections to the two states of $^{15}N$ turns out to be close to the PWIA prediction.

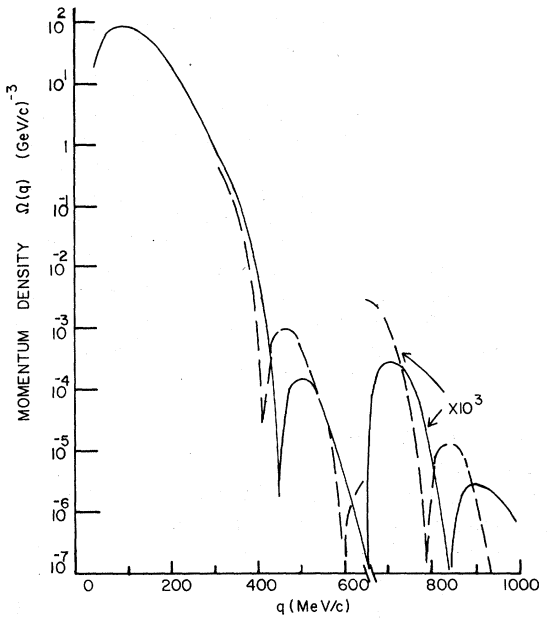


FIG. 18. Single-particle momentum density for $1p_{1/2}$ and $1p_{3/2}$ proton wave functions in $^{16}O$ using the potential of Elton and Swift. Momentum density in $(\text{GeV}/c)^{-3}$ vs momentum in MeV/$c$. For comparison, the $1p_{3/2}$ density has been multiplied by $\frac{1}{2}$; with this normalization, in the absence of spin-orbit splitting the $1p_{3/2}$ and $1p_{1/2}$ momentum densities would be identical. For $q > 660$ MeV/$c$ both momentum densities have been multiplied by 1000.

### B. Center-of-mass corrections for the shell-model wave functions

For our calculations in Sec. IV, we have used expansions of harmonic oscillator wave functions which have not been corrected for center-of-mass effects. The resulting c.m. corrections will apply somewhat differently to the direct and isobar amplitudes. For harmonic oscillator wave functions, the c.m. corrections which occur in direct knock-out reactions have been derived by Dieperink and de Forest.[85] For ejection of a nucleon in the outermost occupied shell state, the c.m. correction involves replacing the momentum at which the single-particle wave function is evaluated by

$$|\vec{p}| \to \left(\frac{A}{A-1}\right)^{1/2} |\vec{q}| . \tag{5.1}$$

In the case of the $^{16}$O photonuclear reaction, this would result in a 3% increase in the momentum component of the single-particle wave function and would correspond to a slight shift of our DWIA curve to the left in Figs. 16 and 17.

In our calculation of the isobar amplitude, we have attempted to account for the c.m. correction arising from the absorption of a pion by the residual nucleus. This is similar to the inclusion of c.m. effects in electromagnetic interactions for inelastic or elastic form factors.[86] For processes in which the c.m. remains in a 1S-state the overall c.m. factors out and the relation between the c.m.-corrected form factor and the uncorrected result is simply an overall multiplicative constant.

$$\rho(\vec{q}) = \exp\left(\frac{q^2 b^2}{4A}\right) \rho_{SM}(\vec{q}) . \tag{5.2}$$

In Eq. (5.2), $q$ is the momentum transfer to the $A$-particle nucleus, $b$ is the oscillator size parameter for the single-particle wave function, $\rho_{SM}(q)$ is the uncorrected shell model form factor, and $\rho(q)$ is the c.m.-corrected form factor. The correction term increases exponentially with the momentum transfer, while the argument of the exponential is inversely proportional to the atomic number of the nucleus.

In order to estimate the importance of c.m. corrections to our single-particle wave functions, we have altered the single-particle transition density $\rho(\vec{q})$, defined from Eq. (4.9), to include the c.m. correction factor of Eq. (5.2). This correction will increase the calculated amplitudes for the isobar term, the increase being the greatest where the momentum transferred by the pion is largest (this will be most apparent where the momentum transferred from photon to nucleon is largest, at the largest laboratory scattering angles for a given photon energy). For these excited nuclear states where the c.m. is not in a 1S state (for example, those states which have holes in deeply bound shells), our correction factor will give an overestimate of the c.m. correction; however, for $^{16}$O these states contribute a reasonably small fraction of the isobar photoexcitation amplitude.

In Figs. 20–22 we show the results of including these c.m. corrections for the $^{16}O(\gamma, p_0)^{15}N$ reactions at scattering angles of 45°, 90°, and 135°. We have included the c.m. correction of Dieperink and de Forest for the direct knock-out amplitude, and the form factor correction of Eq. (5.2) has been included in our isobar calculation. At lower photon energies where the direct term dominates, the effect of the c.m. correction essentially amounts to a slight shift of the theoretical calculation, since it corresponds to evaluating the single-particle momentum at a slightly higher value. The c.m. correction factor increases the theoretical results, although the net increase observed in the cross sections is never greater than a factor of 3 for the energies we have calculated. For photon energies greater than 200 MeV, the cross sections at 90° and 135° are in rather good agreement with experimental data, whereas the 45° cross section is higher than the data by a factor of about 4. As could be expected, the c.m. correction for the isobar term has the greatest effect at the highest photon energies.

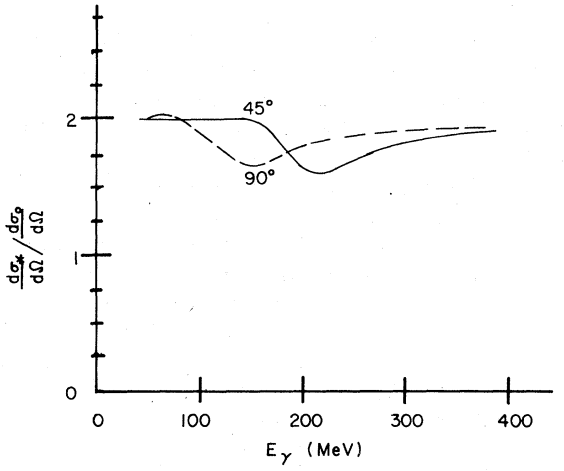


FIG. 19. Ratio $(d\sigma^*/d\Omega)/(d\sigma_0/d\Omega)$ for $(\gamma,p)$ reactions to different states of $^{15}$N, vs photon laboratory incident energy in MeV. $d\sigma^*/d\Omega$ is the $^{16}O(\gamma,p)^{15}N$ cross section leading to the $(\frac{3}{2},-)^{15}N$ state at 6.32 MeV and $d\sigma_0/d\Omega$ is the cross section leading to the $^{15}$N ground state. Solid curve: proton scattering angle of 45° relative to the photon direction; dashed curve: proton scattering angle of 90°.

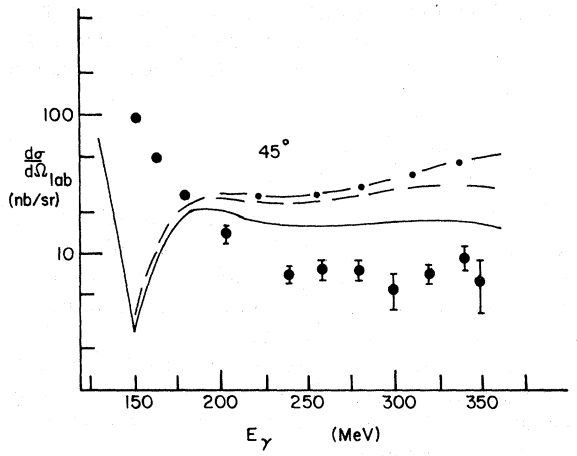


FIG. 20. Lab differential cross sections $d\sigma/d\Omega$ in nb/sr vs photon energy $E_\gamma$ in MeV for the reaction $^{16}O(\gamma,p_0)^{15}N$, at proton lab scattering angle of 45°. Solid curve: distorted-wave results for direct plus isobar amplitudes without including c.m. corrections for single-particle functions. Dashed curve: distorted-wave results including c.m. corrections. The direct term is modified by the prescription of Dieperink and de Forest, Ref. 72, and the single-particle transition density in the isobar amplitude has been multiplied by the c.m. correction factor of Eq. (5.2). The free width (115 MeV) has been used for the isobar. Dot-dashed curve: distorted-wave results including both the c.m. correction and a change in the isobar width to 50 MeV.

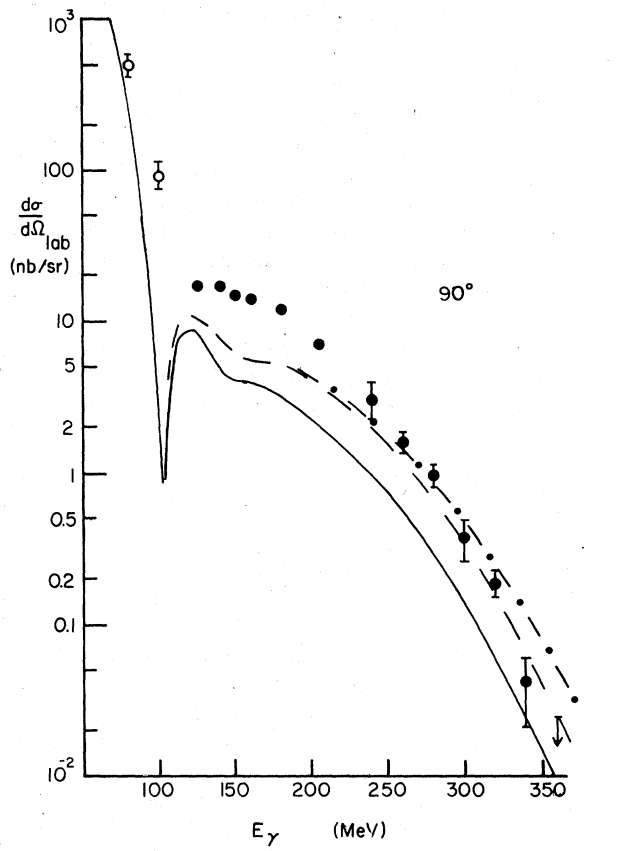


FIG. 21. Lab differential cross sections vs photon energy for $^{16}O(\gamma,p_0)^{15}N$ at proton scattering angle 90°. Notation is that of Fig. 20.

### C. Sensitivity to changes in the isobar width

In our calculation we have neglected the isobar-nucleus interaction, in that we have used the free position and width for the Δ in our propagator. A correct many-body treatment of the isobar-nuclear dynamics would result in the addition of the isobar self energy into the Δ propagator of Eq. (4.1) and subsequent equations. Such a dynamical calculation would result in the replacement of the isobar position and width by an effective position and width for the Δ pole with an explicit dependence on the parametric energy. This point has been emphasized by Brown and Weise[81] in their review of the isobar contribution to pion scattering, and it has been studied in detail by Moniz[87] and Hirata *et al.*[88] in analyses of isobar-hole nuclear dynamics. Moniz has recently suggested that "inclusive" $\gamma$-knock-out experiments summing over nuclear final states might provide detailed information on the isobar-nuclear interaction.[89]

Although we have not included isobar self-energy effects in our calculation, we can demonstrate the sensitivity of our results to shifts in the isobar pole position, in particular to shifts in the isobar width from its free value of 115 MeV. We have recalculated the $(\gamma,p)$ cross sections on $^{16}O$ with the isobar width arbitrarily decreased to $\Gamma = 50$ MeV. These results are plotted as the dot-dashed curves in Figs. 20–22. In calculating these curves we have used distorted waves for the nucleons and we have employed the c.m. corrections discussed in Sec. V B. As a result, the dashed and dot-dashed curves in these figures differ only in the isobar width used. As the isobar width is decreased, the cross sections increase, and the amount of increase in cross sections seems to be a function of the photon energy and relatively independent of scattering angle. For photon energies around 300 MeV, the cross sections calculated with the smaller isobar width begin to be noticeably larger than those using the free width.

The width $\Gamma = 50$ MeV represents a very large decrease from the free width; nevertheless, the resulting cross sections are virtually identical with the calculations using $\Gamma = 115$ MeV, for photon energies below 300 MeV. Although we have not calculated the isobar propagator in the nuclear

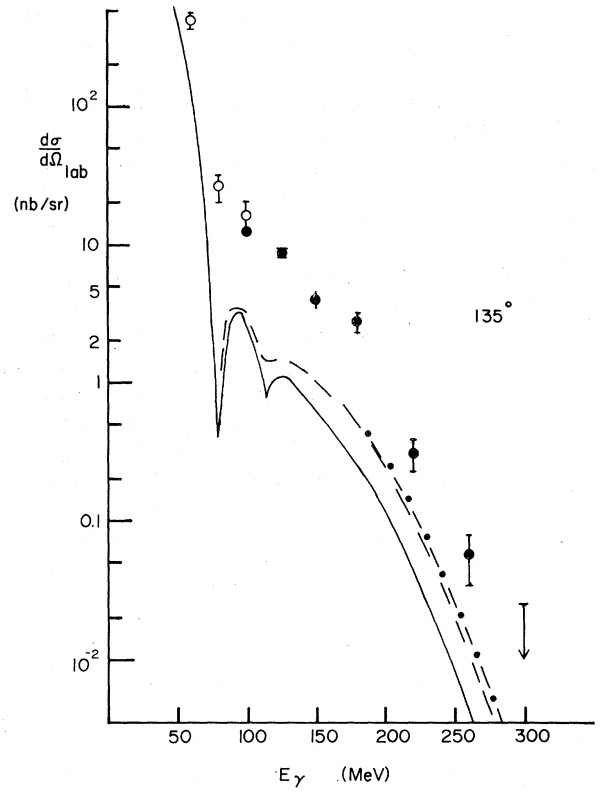


FIG. 22. Lab differential cross section vs photon energy for $^{16}O(\gamma,p_0)^{15}N$ at proton scattering angle 135°. Notation is that of Fig. 20.

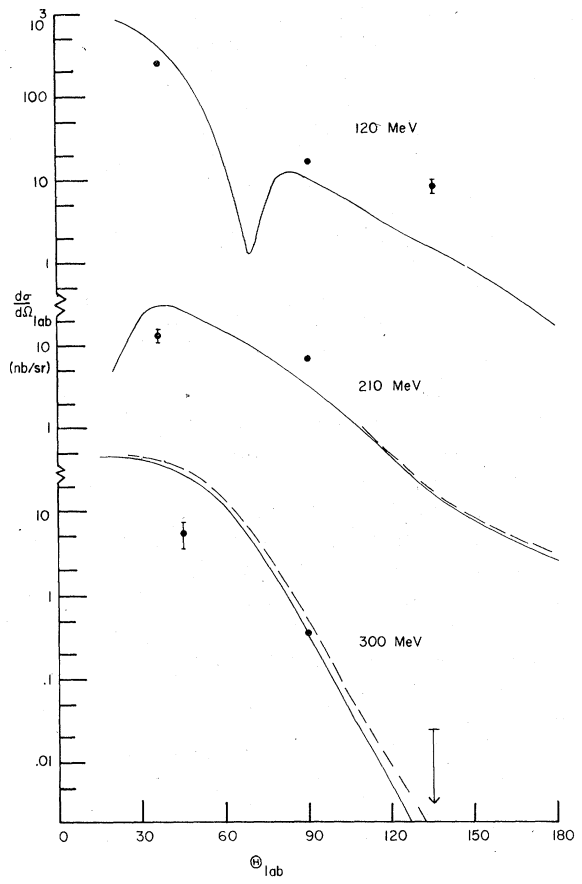


FIG. 23. Laboratory differential cross sections $d\sigma/d\Omega$ in nb/sr vs proton scattering angle $\theta$ (degrees) for photon energies 120, 210, and 300 MeV. Distorted waves for the proton have been used, and c.m. corrections have been applied to the direct and isobar amplitudes. Solid curve: free width of 115 MeV used for the isobar. Dashed curve: width of 50 MeV used for the isobar. Data points are the Bates results at the nearest available photon energies: 126.4, 204.5, and 301.4 MeV, respectively.

medium, and we have not added an energy dependence to the isobar width in the medium, we have shown that (at least for the specific reaction we have examined in detail) the $(\gamma,p_0)$ cross sections do not seem to be strongly dependent upon the isobar width.[90]

We have also plotted the angular distributions at fixed photon energy for three energies, $E_\gamma = 120$, 210, and 300 MeV. These are shown in Fig. 23. The dips in the angular distributions at 70° for $E_\gamma = 120$ MeV and at forward angles for $E_\gamma = 210$ MeV are due to the minimum in the direct amplitude [such a minimum is not seen in lower energy $(\gamma,p)$ measurements]. The isobar contribution predicts a cross section which falls smoothly but rather steeply with increasing angle. In our calculation, all large-angle scattering is dominated by the isobar term. The dashed line in Fig. 23 shows the result of decreasing the isobar width in our calculation to 50 MeV; this has very little effect for photon energies below 300 MeV. The $(\gamma,p)$ cross sections which we calculate are rather forward peaked; they become progressively more forward peaked as the photon energy increases.

### D. Contribution of $\rho$ exchange

In addition to the diagram we have considered, there is an additional diagram in which the $\pi$ meson from the isobar decay is replaced by a $\rho$ meson. Such a diagram is shown in Fig. 24; consideration of this term in our calculation is analogous to including $\rho$ exchange in addition to $\pi$ exchange in the $\Delta N \to NN$ amplitude. Brown and collaborators[81,91] have emphasized repeatedly that the $\rho$ meson can (and probably should) be included in intermediate states whenever the pion can, and there are situations where inclusion of $\rho$ exchange in nucleon and pion scattering problems causes dramatic changes in theoretical amplitudes.[92] In order to show the qualitative influence of $\rho$ ex-

change, we write down the nonrelativistic approximation of the one-pion-exchange (OPE) contribution to the $\Delta N \to NN$ amplitude

$$M^{\mathrm{OPE}}_{\Delta N\to NN} = \frac{-ff^*}{m_\pi^2}\,\frac{\vec{S}^\dagger\cdot q\vec{\sigma}\cdot\vec{q}\,\vec{T}^\dagger\cdot\vec{\tau}}{m_\pi^2 - q_0^2 + |\vec{q}|^2}\,; \tag{5.3}$$

in analogous fashion, we can write the nonrelativistic reduction of the $\rho$-exchange contribution to this amplitude as

$$M\rho_{\Delta N\to NN} = \frac{-f_\rho f_\rho^*}{m_\rho^2}\,\frac{[(\vec{S}^\dagger\cdot\vec{\sigma})\,|\vec{q}|^2 - \vec{S}^\dagger\cdot\vec{q}\vec{\sigma}\cdot\vec{q}]\vec{T}^\dagger\cdot\vec{\tau}}{m_\rho^2 - q_0^2 + |\vec{q}|^2}\,. \tag{5.4}$$

In Eq. (5.4), $f_\rho$ is the $\rho NN$ coupling constant, and $f_\rho^*$ is the $\rho N\Delta$ coupling constant.[93] Comparing Eqs. (5.3) and (5.4), we see that the term in the $\rho$-exchange potential proportional to $\vec{S}^\dagger\cdot\vec{q}\,\vec{\sigma}\cdot\vec{q}$ will tend to cancel the OPE contribution. In the static approximation (a reasonable approximation for our amplitude), for large $|\vec{q}|$ the $\rho$-exchange term can dominate, and in fact can change the sign of this term relative to the OPE case. Since this term goes into making up the $\Delta N \to NN$ "tensor force," then addition of $\rho$ exchange will significantly modify this tensor force; in reactions where the tensor force is very important, inclusion of $\rho$ exchange may give strikingly different results from the OPE predictions.

For our coupling constant $f_\rho$ we could choose from a wide assortment of values in the literature,[94-98] ranging from $f_\rho = 4.82$ to $f_\rho = 8.37$, the latter value given by Hohler and Pietarinen.[98] We obtained $f_\rho^*$ from $f_\rho$ by using the quark model relation derived by Haapakoski[97]

$$f_\rho^* = \tfrac{6}{5}\sqrt{2}\,f_\rho\,. \tag{5.5}$$

In our calculation, we have used the coupling constant of Hohler and Pietarinen; since these are significantly larger than previous estimates of the coupling constant they should give an upper limit to the suppression produced by the addition of $\rho$ exchange. We find that the addition of $\rho$ exchange produces a suppression which is never greater than 30% for photon energies below 350 MeV; for smaller $\rho$ coupling constants the suppression would be proportionately less. In our amplitude, the contribution from large-momentum transfers is suppressed by the single-particle transition densities which become considerably smaller at high-momentum transfers. Thus, the region of high-momentum transfer where $\rho$ exchange would considerably alter the OPE result does not contribute much to our photonuclear amplitude. We note that the $\rho$-exchange term of Eq. (5.4) (in addition to the "tensor force" piece which it has in common with the OPE amplitude), also contains a spin-spin piece proportional to $\vec{S}^\dagger\cdot\vec{\sigma}$. In general this piece would also contribute to the $\rho$-exchange amplitude; however, for our case it is easy to show that, when combined with the photon vertex which has the form $\vec{S}\cdot\vec{\epsilon}^\lambda$, as shown in Eq. (4.6), that the product of these amplitudes vanishes when summed over isobar spins [as can be seen by applying Eq. (4.10)]. Consequently this term contributes nothing to the isobar photonuclear amplitude.

We find the influence of $\rho$ suppression to be rather small for our calculations, even for $\rho$-exchange coupling constants which are considerably larger than previously accepted values. Our results are consequently not altered significantly by this term. However, we should point out that it has been shown by Arima *et al.*[99,100] that nuclear wave functions containing two nucleon correlations induced by the tensor force can give quite different results when one evaluates the matrix elements of pion (and hence also $\rho$) exchange processes. For such correlated wave functions, both the OPE and $\rho$-exchange matrix elements might change significantly and in such systems the suppression from $\rho$ exchange could be considerably greater than that found in our calculation.

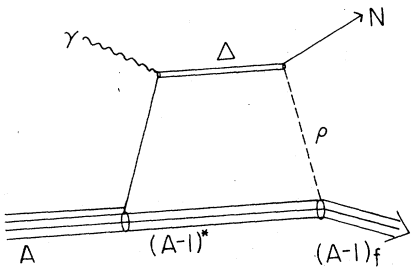


FIG. 24. Contribution to the nuclear photoeffect in which the virtual pion from the isobar decay is replaced by a $\rho$ meson.

## VI. SUMMARY AND CONCLUSIONS

In this paper, we have constructed the isobar amplitude for photonuclear reactions at medium energies. The isobar amplitude gives a large contribution in the energy region 200–400 MeV and in our calculation is the dominant contribution at these energies. Using nuclear wave functions with either short-range correlations or large high-momentum components may give a large cross section for the direct-reaction term (as pointed out by Findlay *et al.*[38-40]); however, since the isobar cross section is qualitatively the same magnitude as the observed cross sections, it must be an important ingredient in any formulation of the nuclear photoeffect at these energies. In our calcu-

lation of $^{16}O$ photodisintegration, the isobar amplitude becomes appreciable for large angle protons (angles greater than or equal to 135°) at photon energies of about 100 MeV, whereas for smaller angles the isobar amplitude does not dominate until photon energies of approximately 250 MeV.

First, we have reviewed the DWIA treatment of medium-energy photonuclear reactions and hence the "direct" photonuclear amplitude. We have included both the convective and magnetic electromagnetic operators, and we have used an optical potential to take into account the distortion of the outgoing proton. We have attempted to include the effects of proton distortion by parametrizing proton scattering wave functions obtained from optical potentials. We find that

(a) the proton wave functions can be rather accurately parametrized by a "modified plane wave" where the real part of the wave number is shifted slightly by the real part of the potential inside the nucleus. Absorption is accounted for in two ways: First, the magnitude of the wave function is decreased due to the loss of flux into inelastic channels. Second, we give the wave functions a (small) imaginary part to the effective momentum, to represent the gradient in the magnitude of the wave function across the nucleus. Of course, the adequacy of such approximations depends upon how accurately they reproduce the same transition amplitude, for $(\gamma,p)$ reactions, as the distorted-wave functions from optical potentials. We are presently investigating this question both for the direct and isobar amplitudes.

(b) For photon energies above 100 MeV, the effects of distortion are *primarily* accounted for by decreasing the magnitude of the proton wave function. Changes in the effective proton wave number become relatively less important at higher energies, because the optical potential strength decreases as the energy increases.

In our calculations, the "direct" term gives the largest contribution to the photonuclear cross section below 100 MeV. We find that the magnetic moment term contributes fairly substantially to the cross sections; since we use an optical potential to account for the proton distortion, we do not find the large suppression of the magnetic term which (as shown by Noble[54]) occurs when the same real potential is used for the binding and scattering potentials. As we have mentioned, it is not clear how much suppression will occur in the magnetic term if one preserves orthogonality while at the same time providing a realistic description of the nucleon-nucleus interaction at medium energies. As we have mentioned, our direct term does not include charge exchange of the outgoing proton or electric exchange-current amplitudes and hence cannot properly reproduce the (experimentally large) $(\gamma,n)$ cross sections.

In calculating the isobar amplitude, we take all coupling constants and widths from independent experiments and we produce a "zero free parameter" calculation of the isobar amplitude which gives a reasonable fit to the existing experimental data. The isobar amplitude has the following features:

(i) It gives a cross section which, for fixed photon energy, is peaked at small angles and which falls rapidly and smoothly with increasing angle.

(ii) The isobar contribution is determined by two terms: the nuclear wave functions, which determine how rapidly this amplitude falls off with increasing scattering angle (for a fixed photon energy); and the isobar propagator which would produce a broad peak in the photonuclear amplitude at a photon energy of about 300 MeV. For $^{16}O(\gamma,p_0)^{15}N$, we can see the relation between these two terms in the calculated cross sections of Figs. 13–15. For small proton scattering angles like 30°, the nuclear form factors are large and relatively constant, so that the theoretical cross section shows a broad peak which is due to the minimum in the isobar propagator. However, for large scattering angles like 135°, the form factors dominate the isobar amplitude; there is no peak in the isobar amplitude, and the theoretical cross section falls smoothly with increasing photon energy. A "break" appears in the cross section at 135° where the isobar contribution becomes large relative to the direct term.

In calculating the isobar contribution to the nuclear photoeffect in other nuclei, the qualitative behavior can be predicted by examining the nuclear form factors relative to the single-particle wave functions for $^{16}O$. If the single-particle wave functions have high-momentum components which are greater than these in $^{16}O$, then the isobar amplitude may produce a peak in the differential cross section around 300 MeV photon energy; however, if the nuclear form factors have much smaller momentum components, then the photodisintegration cross sections may fall rather smoothly with photon energy and show no "obvious" signs of the isobar contribution i.e., no peak in the cross section.

(iii) For the nuclear photoeffect in $^{16}O$, our calculation predicts essentially equal $(\gamma,p)$ and $(\gamma,n)$ cross sections in the region where isobar production is the dominant amplitude. One can excite either a $\Delta^\circ$ or a $\Delta^+$, and each of these can decay to either neutron or proton depending on the charge of the virtual pion. Consequently this would predict roughly equal proton and neutron cross sections at these energies.

(iv) We have estimated the effects of several of

the parameters in our calculation (width of isobar in the nuclear medium, effects of virtual $\rho$ as well as virtual $\pi$ states, and c.m. effects) and found that none of these effects change the *qualitative* features of our calculation (although the detailed results are sensitive in some degree to all of these).

In conclusion, we believe that isobar photoproduction plays an important role in the nuclear photoeffect at medium energies. The high-quality data from Bates on $^{16}$O suggests that this effect is increasingly important at larger photon energies, and that a model which accurately calculates the isobar production and decay (while neglecting the isobar-nucleus dynamics) reproduces the observed features of the experimental data. Further experimental data on other nuclear targets, or perhaps a measurement of certain excited states of the residual nuclei, can help greatly in a quantitative determination of this process.

*Note added in proof.* The $(\gamma,p)$ cross sections on $^{16}$O leading to the $(\frac{3}{2}^-)$ excited state in $^{15}$N have been reported to be about six times greater than the cross section to the $(\frac{1}{2}^-)$ ground state of $^{15}$N [W. Bertozzi, in *Proceedings of the International School on Electro and Photonuclear Reactions*, edited by S. Costa and C. Schaerf (Springer, Berlin, 1977)]. It has been argued by B. Schoch [Phys. Rev. Lett. 41, 80 (1978)] that this value supports a quasideuteron picture of the $(\gamma,p)$ reaction at medium energies.

The authors would like to thank Dr. J. L. Matthews for permission to use preliminary data from Bates and for many stimulating discussions. We would also acknowledge conversations with R. O. Owens, D. J. S. Findlay, and G. E. Walker. One of the authors (J. T. L.) wishes to thank G. E. Brown for stimulating discussions, and P. Schwandt for information and computer programs regarding optical potentials.

## APPENDIX: $\gamma N\Delta$ MATRIX ELEMENT

In this section we review our calculation of the amplitude for photoproduction of the $\Delta(1232)$ isobar from a nucleon. We have taken this amplitude from the work of Thornber,[80] who used a symmetric quark model for the nucleon and isobar to calculate the cross sections for electroproduction of isobars. In this model, the nucleon and isobar are both considered to be combinations of quarks which are completely symmetric under the exchange of any pair. In both the nucleon and isobar, the spatial wave functions are given as a product of $s$-wave Gaussian wave functions for the three quarks; the size parameter $b_Q$ for the wave function is varied to fit the electroproduction data [and was found by Thornber to be equal to $b_Q = 4.0$ (GeV/$c$)$^{-1}$]. The spin-isospin states were then required to be symmetric under exchange.

For a photon of momentum $\vec{k}_\gamma = k_\gamma \hat{z}$ with polarization $\lambda$ along the incident axis, the isobar photoproduction amplitude has the form

$$\langle \Delta, \psi^\alpha_{A-1} | M^\lambda_{\alpha N\Delta} | \psi_A \rangle = -e \sum_{J,M} (i)^J \left[\frac{2\pi(2J+1)}{2k_\gamma}\right]^{1/2} \langle \Delta | \hat{T}^{\rm el}_J(k_\gamma) + \lambda \hat{T}^{\rm mag}_{J,M}(k_\gamma) | \alpha \rangle \varphi_\alpha(\vec{p}_\Delta - \vec{k}_\gamma) , \tag{A1}$$

where $\hat{T}^{\rm el}$ and $\hat{T}^{\rm mag}$ are electric and magnetic multipole single-particle operators, respectively.[85] Equation (A1) is the product of two terms: The first term is the $\gamma N\Delta$ amplitude representing isobar production from a nucleon (i.e., a collection of three quarks), and the second term is the wave function for a single nucleon with quantum numbers $\{\alpha\}$ evaluated at momentum $\vec{p}_\Delta - \vec{k}_\gamma$, $\vec{p}_\Delta$ being the isobar momentum. We have assumed that the residual nucleus with superscript $\alpha$ is obtained by removing a nucleon with quantum numbers $\{\alpha\}$ from the initial state

$$\langle \psi^\alpha_{A-1} \rangle \equiv a_\alpha(p) | \psi_A \rangle ,$$

$a_\alpha$ being the destruction operator for a nucleon with quantum number $\{\alpha\}$, and the single-particle momentum wave function appearing in Eq. (A1) is just the Fourier transform of the bound single-particle wave function

$$\varphi_\alpha(\vec{q}) = \int d^3r e^{-i\vec{q}\cdot\vec{r}} \psi_\alpha(\vec{r}) . \tag{A2}$$

For the case of the $\Delta(1232)$, only the $J=1$ magnetic term survives (owing to parity), so that our amplitude becomes

$$\langle \Delta, \psi^\alpha_{A-1} | M^\lambda_{\gamma N\Delta} | \psi_A \rangle = -ie \left(\frac{3\pi}{k_\gamma}\right)^{1/2} \times \lambda \langle \Delta | \hat{T}^{\rm mag}_{1\lambda}(k_\gamma) | \alpha \rangle \varphi_\alpha(\vec{p}_\Delta - \vec{k}_\gamma) , \tag{A3}$$

where

$$\hat{T}^{\rm mag}_{JM}(q) \equiv \int d^3x \vec{M}^M_{J,J}(\vec{x}) \cdot \hat{J}(\vec{x}) . \tag{A4}$$

In Eq. (3),

$$\vec{M}^M_{J,J}(\vec{x}) \equiv j_J(qx) \sum_{m,m'} \left\langle \begin{matrix} J & 1 \\ m & m' \end{matrix} \middle| \begin{matrix} J \\ M \end{matrix} \right\rangle Y^m_J(\Omega_x) \vec{\epsilon}^{m'} , \tag{A5}$$

and $\hat{J}(\vec{x})$ is the electromagnetic current for the hadrons, expressed as a sum of one-body interactions with the three constituents of the nucleon or isobar,

$$\hat{J}(\vec{x}) = \sum_{j=1} \frac{\hat{Q}(i)}{2iM_q} [\delta(\vec{x} - \vec{r}_j)\vec{\nabla}_x]_{SYM} + \vec{\nabla}x \sum_{j=1} \hat{Q}(j)\mu_p \delta(\vec{x} - \vec{r}_j)\vec{r}(\vec{j}) . \quad \text{(A6)}$$

In Eq. (A6), $M_q$ is the mass of the quark, $\mu_p$ the proton magnetic moment in nuclear magnetons, and $\hat{Q}(j)[\vec{\sigma}(j)]$ is the charge (spin) operator for the $j$th quark. The convective term [the first term in Eq. (A6)] has zero matrix element between nucleon and isobar since it does not change the particle spin. Substituting Eqs. (A5) and (A6) into (A4) and integrating by parts, we obtain

$$\hat{T}^{mag}_{1,\lambda}(k_\gamma) = \left(\frac{2}{3}\right)^{1/2} ik_\gamma \mu_p \int d\vec{x} \sum_{j=1}^{3} \delta(\vec{x} - \vec{r}_j) \times \hat{Q}(j)\vec{M}^{\lambda}_{1,0}(\vec{x})\cdot\vec{\sigma}(j) . \quad \text{(A7)}$$

In Eq. (A7) we have used the fact that all three quarks are in $S$-wave orbits.

It is a straightforward procedure to evaluate the matrix elements of $\hat{T}^{mag}$ between nucleon and isobar states; however, we can dramatically simplify our algebra by writing the matrix elements of $\hat{T}^{mag}$ in terms of the operators $\vec{S}$ and $\vec{T}$. The operator $\vec{S}$ can be written as a matrix which operates between nucleon and isobar spinors; its matrix elements are defined in such a way as to reproduce the matrix elements between isobar and nucleon wave functions; the matrix elements of $S$ are defined as

$$(\vec{S})^{M,m_S} = \sum_{m,\alpha} \left\langle \begin{matrix} 1 & \frac{1}{2} \\ \alpha & m \end{matrix} \middle| \begin{matrix} \frac{3}{2} \\ M \end{matrix} \right\rangle \vec{\epsilon}^{\alpha}(\chi^m_{m_s}) ; \quad \text{(A8)}$$

an analogous equation exists for $T$.[81] It can be shown that an equivalent expression to Eq. (A7) is

$$\hat{T}^{mag}_{1,\lambda}(k_\gamma) = \frac{ik_\gamma \mu_p}{\sqrt{3}\pi} \exp\left(-\frac{k_\gamma{}^2 b_Q{}^2}{6}\right) T_0 \vec{S}\cdot\vec{\epsilon}^{\lambda} . \quad \text{(A9)}$$

In Eq. (A9), $\vec{\epsilon}^{\lambda}$ is the photon polarization vector, and a c.m. correction factor has been removed from the Gaussian form factor for the single-particle wave function. The isobar photoproduction amplitude can then be written

$$\langle \Delta, \psi^{\alpha}_{A-1} | M^{\lambda}_{\gamma N\Delta} | \psi_A \rangle = e\mu_p \sqrt{k_\gamma} \exp\left(-\frac{k_\gamma{}^2 b_Q{}^2}{6}\right) \times \langle \chi_\Delta | T_0 \vec{S}\cdot\vec{\epsilon}^{\lambda} | \chi_\alpha \rangle \varphi_\alpha(\vec{p}_\Delta - \vec{k}_\gamma) . \quad \text{(A10)}$$

In Eq. (A10), $\chi_\Delta$ and $\chi_\alpha$ are the spin-isospin indices for the $\Delta$ and nucleon, respectively. If we apply Eq. (A10) to calculate $\Delta \to N + \gamma$, we can easily calculate the isobar radiative decay width; we find that the width calculated from this formula is somewhat smaller than the experimentally determined value.[44] Consequently, we have multiplied the amplitude of (A9) by 1.33 to correctly reproduce the observed width, and it is this modified amplitude which we have used in our $(\gamma, p)$ calculations.

---

*Supported in part by the National Science Foundation under Grant No. PHY-77-07656 and in part by the United States Department of Energy under Contract No. EY-76-C-02-3069.

†Present address.

[1]T. Kamae, I. Arai, T. Fujii, H. Ikeda, N. Kajiura, S. Kawabata, K. Nakamura, K. Ogawa, H. Takeda, and Y. Watase, Phys. Rev. Lett. 38, 468 (1977). References (1–42) are representative of medium-energy photonuclear experiments and are not intended to be complete.

[2]P. Dougan, T. Kivikas, K. Lunger, V. Ramsay, and W. Stiefler, Z. Phys. A276, 55 (1976).

[3]R. Kose, W. Paul, K. Stockhorst, and K. H. Kissler, Z. Phys. 202, 364 (1967).

[4]J. Buon, V. Gracco, J. Lefrancois, P. Lehmann, B. Merkel, and Ph. Roy, Phys. Lett. 26B, 595 (1968).

[5]R. L. Anderson, R. Prepost, and B. H. Wiik, Phys. Rev. Lett. 22, 651 (1969).

[6]A. M. Smith, S. J. Hall, B. Mann, and D. T. Stewart, J. Phys. A 1 (Proc. Phys. Soc.), 553 (1968).

[7]D. I. Sober, D. G. Cassel, A. J. Sadoff, K. W. Chen, and P. A. Crean, Phys. Rev. Lett. 22, 430 (1969).

[8]R. Ching and C. Schaerf, Phys. Rev. 141, 1320 (1966).

[9]T. A. Gabriel and R. B. Alsmiller, Jr., Phys. Rev. 182, 1035 (1969).

[10]P. Picozza, C. Schaerf, R. Scrimaglio, G. Goggi, A. Piazzoli, and D. Scannicchio, Nucl. Phys. A157, 190 (1970).

[11]J. P. Didelez, H. Langevin-Joliot, Z. Maric, and V. Radojevic, Nucl. Phys. A143, 602 (1970).

[12]A. van der Woude, M. L. Halbert, C. R. Bingham, and B. D. Belt, Phys. Rev. Lett. 26, 909 (1971).

[13]N. M. O'Fallon, L. J. Koester, Jr., and J. H. Smith, Phys. Rev. C 5, 1926 (1972).

[14]G. Ticcioni, S. M. Gardiner, J. L. Matthews, and R. O. Owens, Phys. Lett. 46B, 369 (1973).

[15]P. E. Argan, G. Audit, N. De Botton, J. L. Faure, J. -M. Laget, J. Martin, C. G. Schuhl, and G. Tamas, Nucl. Phys. A237, 447 (1975).

[16]C. A. Heusch, R. V. Kline, K. T. McDonald, and C. Y. Prescott, Phys. Rev. Lett. 37, 405 (1976).

[17]C. A. Heusch, R. V. Kline, K. T. McDonald, J. B.

Carroll, D. H. Frederickson, M. Goitein, B. Macdonald, V. Perez-Mendez, and A. W. Stetz, Phys. Rev. Lett. 37, 409 (1976).
[18]D. Bachelier, M. Bernas, I. Brissaud, C. Detraz, H. Langevin-Joliot, J. Lee, and P. Radvanyi, Phys. Lett. 21, 697 (1966).
[19]J. P. Didelez, H. Langevin-Joliot, N. Bijedic, and Z. Maric, Nuovo Cimento 67A, 388 (1970).
[20]A. N. Gorbunov, Zh. Eksp. Teor. Fiz. Pis. Red. 8, 148 (1968) [Sov. Phys. JETP Lett. 8, 88 (1968)].
[21]M. Arkatov, P. I. Vatset, V. I. Volshchuk, V. V. Kirichenko, I. M. Prokhorets, and A. F. Khodyachikh, Yad. Fiz. 12, 227 (1970) [Sov. J. Nucl. Phys. 12, 123 (1971)].
[22]A. N. Gorbunov, Phys. Lett. 27B, 436 (1968).
[23]E. B. Bazhanof and L. A. Kul'chitskii, Zh. Eksp. Teor. Fiz. 38, 1685 (1960) [Sov. Phys.—JETP 11, 1215 (1960)].
[24]J. L. Matthews, W. Bertozzi, S. Kowalski, C. P. Sargent, and W. Turchinetz, Nucl. Phys. A112, 654 (1968).
[25]D. J. S. Findlay, thesis, University of Glasgow, 1975 (unpublished).
[26]S. N. Gardiner, J. L. Matthews, and R. O. Owens, Phys. Lett. 46B, 186 (1973).
[27]M. Sanzone, G. Ricco, S. Costa, and L. Ferrero, Nucl. Phys. A153, 225 (1969).
[28]C. Whitehead, W. R. McMurray, M. J. Aitken, N. Middlemas, and C. H. Collie, Phys. Rev. 110, 941 (1955).
[29]H. Langevin-Joliot, C. Stephan, G. Johnson, and J. Vernotte, Phys. Lett. 14, 208 (1965).
[30]S. Penner and J. E. Leiss, Phys. Rev. 114, 1101 (1959).
[31]G. Manuzio, G. Ricco, M. Sanzone, and L. Ferrero, Nucl. Phys. A133, 225 (1969).
[32]G. G. Taran and A. N. Gorbunov, Yad. Fiz. 6, 1124 (1967) [Sov. J. Nucl. Phys. 6, 816 (1968)].
[33]H. G. Miller, W. Buss, and J. A. Rawlins, Nucl. Phys. A163, 637 (1971).
[34]H. Schier and B. Schoch, Nucl. Phys. A229, 93 (1974).
[35]E. Mancini, G. Ricco, M. Sanzone, S. Costa, and L. Ferrero, Nuovo Cimento 15A, 705 (1973).
[36]A. N. Gorbunov and V. A. Osipova, Zh. Eksp. Teor. Fiz. 43, 40 (1962) [Sov. Phys.—JETP 16, 27 (1963)].
[37]J. L. Matthews, D. J. S. Findlay, S. N. Gardiner, and R. O. Owens, Nucl. Phys. A267, 51 (1976).
[38]D. J. S. Findlay and R. O. Owens, Nucl. Phys. A279, 385 (1977).
[39]D. J. S. Findlay and R. O. Owens, Nucl. Phys. A292, 53 (1977).
[40]D. J. S. Findlay and R. O. Owens, Phys. Rev. Lett. 37, 674 (1976).
[41]J. L. Matthews, W. Bertozzi, M. J. Leitch, C. A. Peridier, B. L. Roberts, C. P. Sargent, W. Turchinetz, D. J. S. Findlay, and R. O. Owens, Phys. Rev. Lett. 38, 8 (1977).
[42]D. J. S. Findlay, R. O. Owens, M. J. Leitch, J. L. Matthews, C. A. Peridier, B. L. Roberts, and C. P. Sargent, Phys. Lett. 74B, 305 (1978).
[43]J. L. Matthews, private communication.
[44]For a review of isobar properties, see T. G. Trippe, A. Barbaro-Galtieri, R. L. Kelly, A. Rittenberg, A. H. Rosenfeld, G. P. Yost, N. Barash-Schmidt, C. Bricman, R. J. Hemingway, M. J. Losty, M. Roos, V. Chaloupka, and B. Armstrong, Rev. Mod. Phys. 48, 2 (1976).
[45]Yu. I. Titov, E. V. Stepula, N. G. Afanas'ev, R. V. Akhmerov, S. A. Byvalin, N. F. Severin, and E. M. Smelov, Yad. Fiz. 13, 1149 (1971)[Sov. J. Nucl. Phys. 13, 660 (1971)].
[46]E. J. Moniz, Phys. Rev. 184, 1154 (1969); E. J. Moniz, I. Sick, R. R. Whitney, J. R. Ficenec, R. D. Kephart, and W. P. Trower, Phys. Rev. Lett. 26, 445 (1971).
[47]T. W. Donnelly and J. D. Walecka, Ann. Rev. Nucl. Sci. 25, 329 (1976).
[48]J. T. Londergan, G. D. Nixon, and G. E. Walker, Phys. Lett. 65B, 427 (1976) (hereafter called I).
[49]I. E. McCarthy, Nucl. Phys. 11, 574 (1959); I. E. McCarthy and D. L. Pursey, Phys. Rev. 122, 578 (1961).
[50]In this paper we use units such that $\hbar = c = 1$; also we use normalized units for the charge $e^2/4\pi = \alpha = \frac{1}{137}$.
[51]We are in an energy region where it makes little sense to use c.m. effective charges derived from long wave length limits. Even if we were to use such effective charges, the resulting neutron effective charge would be extremely small, as the neutron effective charge for electric multipoles goes like $Z(-1/A)^L$. At these high energies, the electric dominant multipole $L$ is greater than 2, which would produce a negligibly small neutron effective charge.
[52]There is an additional recoil contribution, primarily to the $(\gamma,n)$ reaction, in which a proton absorbs the photon and a neutron is ejected. This gives rise to a backward-peaked neutron cross section; as we shall mention, the PWIA $(\gamma,n)$ cross sections do not reproduce the experimental data, which is as large (to within a factor of 2) as the $(\gamma,p)$ data and is relatively forward peaked. We have not included the recoil contribution to the $(\gamma,n)$ cross sections.
[53]In the PWIA analysis, the orthogonality of the initial- and final-state wave functions is not respected. It has been pointed out (Ref. 54) that a treatment of the nuclear photoeffect which respects wave function orthogonality may dramatically decrease the magnetic cross section from the PWIA prediction. This point is not completely certain, and it is discussed further in Sec. III B; however it is possible that the magnetic cross section predicted by the PWIA is considerably larger than the "correct" magnetic contribution.
[54]J. V. Noble, Phys. Rev. C 17, 2151 (1978)
[55]The normalization of $\Omega(q)$ is chosen so that $\Omega(q)$ is equal to $(1/4\pi)|Q_l(q)|^2$, the "momentum density" defined by Findlay and Owens (Refs. 38–40, 42). Our wave functions are normalized to 1, i.e.,

$$\int \frac{d^3q}{(2\pi)^3} |\varphi_{nljm}(\vec{q})|^2 = 1 .$$

[56]T. W. Donnelly and G. E. Walker, Phys. Rev. Lett. 22, 1121 (1969).
[57]L. R. B. Elton and A. Swift, Nucl. Phys. A94, 52 (1967).
[58]J. W. Negele, Phys. Rev. C 1, 1260 (1970).
[59]H. K. Lee and H. McManus, Phys. Rev. 161, 1087 (1977).
[60]D. F. Jackson and L. R. B. Elton, Nucl. Phys. 43, 136 (1963); D. F. Jackson, *ibid.* 54, 561 (1964); D. F. Jackson and T. Berggren, *ibid.* 62, 353 (1965).
[61]N. Austern, *Direct Reaction Nuclear Theories* (Wiley-Interscience, New York, 1970), Chap. 7.
[62]The optical potential parameters $V = 50$ MeV, $W = 6$ MeV (volume absorption), $r_0 = 1.2$ fm, and $a = 0.55$ fm, were

those used by K. Amos [Nucl. Phys. 77, 225 (1966)], in his study of nucleon distortion effects at low energies.
[63]G. Satchler and R. Haybron, Phys. Lett. 11, 313 (1964).
[64]C. M. Perey and F. G. Perey, At. Data Nucl. Data Tables 17, 1 (1976).
[65]G. Passatore, Nucl. Phys. A95, 694 (1967).
[66]G. Passatore, Nucl. Phys. A248, 509 (1975).
[67]P. E. Hodgson, *Nuclear Reactions and Nuclear Structure*, (Oxford U. P., London, 1971).
[68]We have previously mentioned that absorptive effects in the nucleon wave functions are reflected in both $\xi$ and $\overline{W}$; consequently it does not make sense to compare our value of $\overline{W}$ with the imaginary potential found by Passatore, except to note that both values increase rather steadily with increasing proton energy. By the same argument, negative values of $\overline{W}$ in our parametrization do not necessarily imply an "emissive" optical potential.
[69]Findlay *et al.* have also used a modified plane-wave approximation for their distorted waves. There are several differences between our approach and theirs. First, we have fitted the wave functions generated from optical potentials while Findlay *et al.* have fitted to the central well depth $V$ as compiled by Passatore; their parametrization corresponds to setting $\overline{W}=0$ in Eq. (3.3), and their fit to $V$ is somewhat different from our fit. Also, they have not included the magnetic moment term in their photonuclear calculations.
[70]J. Mougey, M. Bernheim, A. Bussiere, A. Gillebert, Phan Xuan Hô, M. Priou, D. Royer, I. Sick, and G. J. Wagner, Nucl. Phys. A262, 461 (1976).
[71]S. Cotanch, Phys. Lett. 76B, 19 (1978).
[72]M. Gari and H. Hebach, Phys. Lett. 49B, 29 (1974); M. Gari and H. Hebach, Phys. Rev. C 10, 1629 (1974).
[73]H. Hebach, A. Wortberg, and M. Gari, Nucl. Phys. A267, 425 (1976); H. Hebach, *Photonuclear Reactions*, in Proceedings of the International School of Electro- and Photonuclear Reactions, Erice, Italy, 1976, edited by S. Costa and C. Schaerf (Springer-Verlag, Berlin, 1977).
[74]Gari and Hebach (Refs. 72 and 73) include electric exchange currents which are very important for photon energies up to 140 MeV. We would expect the isobar effects to dominate over the other pionic exchange currents at higher photon energies, and this result is obtained by Gari and Hebach who have estimated these exchange current terms at higher energies (M. Gari and H. Hebach, Report, 1978) (unpublished).
[75]M. Fink, H. Hebach, and K. Kummel, Nucl. Phys. A186, 353 (1972).
[76]M. Gourdin and Ph. Salin, Nuovo Cimento 27, 193 (1963); M. Gourdin and Ph. Salin, *ibid.* 27, 300 (1963).
[77]B. H. Brandsden and R. G. Moorhouse, *The Pion-Nucleon System*, (Princeton U.P., Princeton, N.J., 1973).
[78]For our calculation we will want to describe both the $^{15}$N ground state and the 6.32 MeV $(\frac{3}{2},-)$ state in $^{15}$N as one-hole states built on $^{16}$O. Detailed shell model calculations of $^{16}$O (Ref. 79) show that the $^{15}$N ground state is well described as a one-hole state relative to $^{16}$O.
[79]A. P. Zuker, B. Buck, and J. B. McGrory, Phys. Rev. Lett. 21, 39 (1968).
[80]N. S. Thornber, Phys. Rev. 169, 1096 (1968).
[81]G. E. Brown and W. Weise, Phys. Rep. 22, 279 (1975).
[82]W. A. Mann, U. Mehtani, B. Musgrave, Y. Oren, P. A. Schreiner, R. Singer, H. Yuta, R. Ammar, S. Barish, Y. Cho, M. Derrick, R. Engelmann, and L. G. Hyman, Phys. Rev. Lett. 31, 844 (1973).
[83]P. A. Schreiner and F. von Hippel, Phys. Rev. Lett. 30, 339 (1973).
[84]Since the isobar current amplitude depends on the low-momentum components of the nuclear wave functions (relative to the direct knock-out term), we should obtain essentially identical results for the isobar amplitude using either Negele's exact single-particle wave functions or the oscillator expansion of these wave functions.
[85]A. E. L. Dieperink and T. de Forest, Phys. Rev. C 10, 543 (1974).
[86]T. de Forest and J. D. Walecka, Adv. Phys. 15, 1 (1966).
[87]E. J. Moniz, in *Meson-Nuclear Physics*—1976, proceedings of the International Topical Conference, Pittsburgh, edited by P. D. Barnes, R. A. Eisenstein, and L. S. Kisslinger (AIP, New York, 1976).
[88]M. Hirata, F. Lenz, and K. Yazaki, Ann. Phys. (N.Y.) 108, 116 (1977).
[89]E. J. Moniz, paper contributed to the M.I.T. Workshop on Nuclear Physics with Electron Accelerators, 1977 (unpublished).
[90]As we have emphasized, the isobar contribution depends upon both the nuclear wave functions and the isobar propagator. If the nuclear wave functions had larger high-momentum components than those we have used, then we would expect the isobar contribution to be more sensitive to changes in the isobar width.
[91]G. E. Brown, in *Meson-Nuclear Physics—1976*, proceedings of the International Topical Conference, Pittsburgh, edited by P. D. Barnes, R. A. Eisenstein, and L. S. Kisslinger (AIP, New York, 1976).
[92]D. O. Riska, M. Brack, and W. Weise, Phys. Lett. 61B, 41 (1976).
[93]Our coupling constant is related to the coupling constants of Brown and Weise by

$$f_\rho = g_\rho (1+\kappa_V)\frac{m_\rho}{2M_N}\sqrt{4\pi} \quad .$$

[94]For a review of the one-boson-exchange model, see K. Erkelenz, Phys. Rep. 13, 191 (1974); also K. Erkelenz, K. Holinde, and K. Bleuler, Nucl. Phys. A139, 308 (1969); K. Holinde, K. Erkelenz, and R. Alzetta, *ibid.* A194, 161 (1972).
[95]A. Gersten, R. Thompson, and A. E. S. Green, Phys. Rev. D 3, 2076 (1971).
[96]G. Schierholz, Nucl. Phys. B40, 335 (1972).
[97]P. Haapakoski, Phys. Lett. 48B, 307 (1974).
[98]G. Höhler and E. Pietarinen, Nucl. Phys. B95, 210 (1975).
[99]A. Arima, G. E. Brown, H. Hyuga, and M. Ichimura, Nucl. Phys. A205, 27 (1973).
[100]W. T. Weng, T. T. S. Kuo, and G. E. Brown, Phys. Lett. 46B, 329 (1973).